HHMI Author Manuscript
HHMI Author Manuscript
HHMI Author Manuscript
PubMed Central
HHMI
HOWARD HUGHES MEDICAL INSTITUTE
AUTHOR MANUSCRIPT
Accepted for publication in a peer-reviewed journal

Published as: *J Neurosci*. 2013 June 5; 33(23): 9813–9830.

# Decorrelating actions of inhibition in neocortical networks

**Tanya Sippy** and **Rafael Yuste**
HHMI, Department of Biological Sciences, Columbia University, New York, NY 10027 USA

## Abstract

Although inhibitory interneurons have been extensively studied, their contribution to circuit dynamics remain poorly understood. While it has been suggested that interneurons, especially those belonging to the same subclass, synchronize their activity and impart this synchrony onto their local network, recent theoretical and experimental work have begun to challenge this view. To better understand the activity of inhibitory interneurons during cortical activity, we combined molecular identification of interneurons, two photon imaging and electrophysiological recordings in thalamocortical slices from mouse somatosensory cortex. Using calcium imaging to monitor cortical activity, we found low spiking correlations among parvalbumin or somatostatin interneurons during cortical UP states, indicating that interneurons do not synchronize their firing. Intracellular recordings confirmed that nearby interneurons do not display more synchronous spiking than excitatory cells, suggesting that their coupling does not function to synchronize their activity. The lack of interneuron synchrony was also evident during slow oscillations, and among interneurons that were electrically coupled via gap junctions. Using voltage clamp recordings from nearby pyramidal cells, we found that inhibitory currents (IPSCs) are more correlated than excitatory ones, but that correlated IPSCs arise from the activation of common presynaptic inhibitory cells, rather than from synchronization of interneuron activity. Finally, we demonstrate that pharmacologically reducing inhibitory currents increases correlated excitatory activity. We conclude that inhibitory interneurons do not have synchronous activity during UP states, and speculate that their function may be to decorrelate rather than synchronize the firing of neurons within the local network.

## Introduction

Information coding in neural networks depends crucially both on the rate of action potential firing (rate code) and the precise timing of spikes (temporal code) across population of neurons. This code is not just the property of a single neuron, which by itself has limited capacity to carry information. Instead, the relevant computations to explain perception or behavior must be a property of the simultaneous functioning of many neurons (McClurkin et al., 1991). In fact, synchrony, the most basic temporal relationship among two or more neurons, has been widely observed in the CNS. Different modes of synchrony have been described both *in vitro* and *in vivo*, and are thought to play a role in development, sensory perception, motor control and other forms of cognition such as attention (Bruno, 2011; Gordon, 2011; Sanes, 2003; Uhlhaas et al., 2010).

Based on many studies in both cortex and hippocampus it is widely accepted that inhibitory transmission is necessary for many forms of synchronous activity (Bartos et al., 2002). Mechanistically, it is known that interneurons that belong to the same subtype are commonly electrically coupled (Galarreta and Hestrin, 1999; Gibson et al., 1999), and this is

Corresponding author: Rafael Yuste, 901 West 120th St. New York, NY 10027, rmy5@columbia.edu.
The authors declare no competing financial interests.

HHMI Author Manuscript
HHMI Author Manuscript
HHMI Author Manuscript



thought to lead to synchronous activity (Gentet et al., 2010), and to promote neuronal oscillations (Deans et al., 2001; Gibson et al., 2005; Kaminski et al., 2011). Nevertheless, most studies focusing on coupling of interneurons examined at most two neurons in very close proximity (within 200 μm), and it is unclear how such coupling affects spiking of larger populations within and beyond these distances. Moreover, interneurons that normally display correlated firing in cerebellum, can become rapidly and strongly desynchronized in response to synaptic inputs and impart this desynchronization onto the local network (Vervaeke et al., 2010).

We investigated the function of subpopulations of interneurons, and address what effect inhibition has on activity of excitatory cells within local circuits. For this task, we chose to use a thalamocortical slice preparation in which recurrent cortical activity (UP states) can be thalamically triggered, or occur spontaneously, either in individual events, or in an oscillatory fashion. We find, first, that inhibitory interneurons, even those that belong to the same cell class (parvalbumin or somatostatin) do not have more correlated activity than their excitatory counterparts. Second, even among electrically coupled inhibitory interneurons, spiking is not synchronous during spontaneous and evoked cortical activity. Third, although isolated inhibitory postsynaptic currents (IPSCs) are more correlated than excitatory postsynaptic currents (EPSCs), this can be explained by the firing of individual interneurons that are presynaptic to neighboring pyramidal cells, rather than by synchronized firing. Finally, a mild pharmacological reduction of inhibition can significantly increase excitatory correlations. Taken together these results provide evidence that interneurons belonging to the same cell class do not coordinate their firing, and open the possibility of other functions of inhibitory neurons other than synchronization of the network.

## Materials and Methods

### Slice preparation

Thalamocortical slices, 400 μm thick, were prepared from postnatal day 13 (P13) to P18, or p28-35 (as indicated in text) from GIN (Oliva et al., 2000) or G42 (Chattopadhyaya, 2004) transgenic mice of either sex, as previously described (MacLean et al., 2005). Slices were cut with a vibratome (VT1200S; Leica, Nussloch, Germany or Microm 650V, ThermoFisher Scientific, Kalamazoo, Michigan) in ice-cold oxygenated modified ACSF that included 0.5 mM CaCl and 3.5 mM $MgSO_4$, in which NaCl was replaced by an equimolar concentration of sucrose. Experiments were performed with ACSF containing (in mM) 123 NaCl, 3 KCl, 26 $NaHCO_3$, 1 $NaH_2PO_4$, 2 $CaCl_2$, 2 $MgSO_4$ and 10 dextrose, which was continuously aerated with 95% $O_2$, 5% $CO_2$ and perfused over the slice at high perfusion rates (125–175 ml/hour)In a subset of experiments, the ACSF was modified to include 1.2mM $CaCl_2$ and 1.0mM $MgSO_4$ and either 3.5mM KCl or 5.0mM KCl. For experiments using gabazine, 100–200nm concentrations were used.

### Electrophysiology

Thalamocortical projection neurons were activated using bipolar platinum-iridium electrodes (#CE2C55, Frederick Haer Co., Bowdoinham, ME) placed in the ventrobasal nucleus (VB) of the thalamus. Stimuli were 200 μs in duration, 20–100 μA in amplitude and were applied individually or as a train of 4–8 stimuli, each separated by 25 ms (40 Hz) using a Master 8 pulse generator coupled to a Iso-flex stimulator (AMPI, Jerusalem, Israel). For each slice the minimal pulse amplitude necessary to evoke recurrent activity was used which allowed us to minimize potential activation of corticothalamic neurons (Agmon and Connors, 1991; Ferster and Lindstrom, 1985). All recordings were made at 33ºC. Calcium imaging of populations of neurons (Yuste and Katz, 1991) was used to identify online responding cells in layer 2/3 and these neurons were then targeted for whole-cell recording.

HHMI Author Manuscript HHMI Author Manuscript HHMI Author Manuscript

Whole-cell current-clamp recordings using Multiclamp 700B amplifiers (Axon Instruments, Foster City, CA) were made from neurons in layer 4 using 4–6 M micropipettes, filled (in mM): 130 K-methylsulfate, 2 $MgCl_2$, 0.6 EGTA, 10 HEPES, 4 ATP-Mg, and 0.3 GTP-Tris, pH 7.2 (290–295 mOsm). To characterize neurons, 500–1000 ms depolarizing DC current injections were given to each cell and resultant action potential firing patterns were analyzed, following the Petilla convention nomenclature (Ascoli et al., 2008).

## Morphological processing

Neurons were filled with biocytin by diffusion from the intrapipette solution during recordings, with electrodes containing 0.4 g/100ml biocytin in addition to the solution described above. At the end of each recording, slices were fixed overnight in 4% paraformaldehyde. Thereafter, slices were rinsed several times in 0.12 M phosphate buffer saline (PB). Slices were then transferred to 30% sucrose in 15 mL of 0.12M PB for at least 2 hours and as long as one week. Slices were then frozen in an embedding medium. After freezing, slices were rinsed in 0.12M PB several times. Slices were then incubated in 1% $H_2O_2$ in 0.12M PB for 30 minutes under agitation and rinsed in 0.12M PB once for 15 minutes. After two other washes in 0.02M KPBS, the slices were incubated overnight under agitation in 1% Avidin-Biotin Complex (ABC Kit Standard, Vector Laboratories) prepared in 0.3% Triton X-100. After three rinses in phosphate buffer, biocytin was revealed by diaminobenzidine. After two final rinses in phosphate buffer, slices were mounted onto slides. The neurons were reconstructed with Neurolucida (Micro Bright Field Inc., USA).

## Antibody labeling

Anesthetized mice (p14) were perfused transcardially with 4% paraformaldehyde in 0.1M phosphate buffer, pH 7.4. A vibratome (Leica VT1000s) was used to cut 50-μm thick coronal sections from somatosensory cortex. Sections were blocked in 10% NDS for 1hr at RT, then incubated 48hrs at RT with primary antibodies: polyclonal rabbit anti-PV (1:1000, Swant PV25) and goat anti-GFP (1:3000, Abcam 5450) in 5% NDS and 0.3% Triton. Subsequently, sections were incubated with anti-rabbit CY3 IgG (1: 500; Jackson ImmunoResearch) and anti-goat Alexa488 (Invitrogen) and mounted.

Images from layer 2/3-5 of S1 were acquired using 20X air objective with a confocal microscope (Zeiss 700 LSM). No bleed through between 488 and 555 channels was observed. Scans were collected in sequential mode and later merged. Images were saved as TIF files and analyzed with MacBioPhotonics ImageJ.

## Calcium indicator bulk loading and imaging

Slices were bulk loaded with Fura 2-AM for visualization of action potential-related activity in neuronal somata. Slices were placed onto the bottom of a small Petri dish (35 × 10 mm) filled with a vortexed mixture of 2 ml ACSF, an aliquot of 50 μg Fura 2-AM (Molecular Probes), 15 μl DMSO and 2 μl Pluronic F-127 (Molecular Probes). A cover was placed over the petri dish and it was incubated in the dark at 35–37 °C and oxygenated by puffed CO2/ O2 gas for ~25 minutes. In order to locate regions in the cortex connected to the area of thalamus we stimulated, we first imaged at low (4X) magnification. Barrels were identified in bright field as repeating ‘hollow rectangles’, corresponding to regions of high cell density, occurring in layer 4, as confirmed with cytochrome oxidase staining (e.g (Feldmeyer et al., 1999). The region in the barrel fields which responded earliest to stimulation was then chosen for higher cell resolution imaging and patch clamping.

Changes in intracellular free $Ca^{2+}$ were visualized with a high numerical aperture 20x (NA, 0.95) Olympus Plan FL objective with an upright fluorescence microscope (Olympus BX50WI; Olympus Optical, Tokyo, Japan) using a Ti:sapphire laser (Chameleon Ultra II,

HHMI Author Manuscript HHMI Author Manuscript HHMI Author Manuscript

Coherent, >3 W, 140 fs pulses, 80 MHz repetition rate) tuned to either 790 (fura-2 AM imaging) or 900nm (GFP imaging). A Hamamatsu C9100-12 (Bridgewater, NJ) camera and Micro-Manager (Vale Lab, UCSF) and ImageJ software (a public domain, Java-based image processing program developed at the National Institutes of Health) were used for targeting neurons for imaging activity from populations of neurons. Frames were acquired at 15–15.67ms/frame. Binning was performed such that images were 256×256 pixels. Files were saved as multipage TIFF stacks.

First, a slow raster scan was performed at a low frame rate (1Hz) to identify cell bodies. In G42 and GIN transgenic knockin mice, the GABAergic GFP labeled interneurons were excited at 900nm. Subsequently, the same field was imaged at 790nm to visualize loaded cell bodies. After these imaged were acquired with the camera, neurons were targeted for imaging on their cell bodies, using a spatial light modulator (SLM). We use a model 1080P phase SLM from Holoeye (Berlin, Germany), which has a resolution of 1920 × 1080 pixels, and an 8-bit phase quantization, with a 60-Hz refresh rate. Patterns were generated with software from Holoeye. In our microscope, collimated light from our laser passes through an optional Pockels cell, which regulates total power, and after beam reshaping and resizing, hits the reflective SLM. A system of lenses relays the image of the SLM surface to the back aperture of the main microscope objective. Some small fraction (<25%) of the incoming light remains undiffracted this is the “zero-order” beam. We used an “on-center” configuration wherein the non-diffracted beam is present in the FOV, and we employ a small beam-stop to remove it.

## Image analysis

To detect calcium signals from imaged cells, loaded neurons were automatically identified using a custom written ImageJ plug-in (written by TA Machado) on the raw image of the slice, and then the fluorescence of these cells was measured as a function of time. All remaining image processing was carried out using custom written software in MATLAB (The MathWorks, Inc., Natick MA).

Fluorescence traces were then preprocessed. Because some slow drift was sometimes present in the traces, each trace was Fourier transformed, and all frequencies <0.5 Hz were set to zero (0.5 Hz was chosen by eye); the resulting fluorescence trace was then normalized to be between zero and one. Taking advantage of the high temporal resolution of our data, we employed a fast nonnegative deconvolution algorithm (Vogelstein et al., 2010) to infer the approximately most likely spike train underlying our fluorescence data. Briefly, the algorithm uses a model that assumes somatic fluorescence arising from the calcium indicator can be approximated by convolving the neuron’s spike train with an exponentially decaying kernel. Noise is assumed to be gaussian, and the spike train is assumed to be poisson. Given this model, and assuming the poisson spike train can be well approximated as an exponential, a convex objective function can be derived. The objective function was numerically optimized given a non-negativity constraint on the spike train implemented using a barrier term. Parameters were manually determined and not estimated from the data. Spike trains were deconvolved from all putative neurons with at least a 5% $\Delta F/F$ change within one movie we stored them in a matrix Finally, we correlated the vectors, each representing the estimated spike train from a single contour, using the MATLAB built in function CORRCOEF.

Although fura 2-AM preferentially labels neurons, any contour with long rise times (> 2 frames), and slow decay times, typical of astrocyte calcium signaling were excluded from the analysis.

HHMI Author Manuscript
HHMI Author Manuscript
HHMI Author Manuscript



### Electrophysiology analysis

UP states were detected automatically (based on an algorithm written by BO Watson) from whole cell current clamp traces based on fulfillment of the following minimum criteria: at least 500 ms of depolarization of 3 mV or more and at least 3 action potentials during this depolarization. If the neuron did not fire action potentials, a continuous depolarization of 5 mV for a minimum of 500 ms was required. This allowed us to detect all UP states despite the variability of membrane behavior exhibited by different neurons. Simultaneous patch clamp recordings confirmed that these criteria allowed for the reliable detection of network UP state events which occurred simultaneously in simultaneously recorded cells. Further, after automatic detection, all events meeting these requirements were reviewed by the experimenter and could be rejected at that point. Durations and amplitudes for verified UP states were quantified based on automatically detected UP state start times and stop times. Action potentials were detected based on their amplitudes and durations and numbers within detected UP states were quantified.

Cross-correlograms and were computed using MATLAB 7.11.0 (MathWorks www.mathworks.com). Shufflegrams were computed by correlating each UP state segment with a randomly selected UP state segment in the same cell without replacement. For calculation of correlations, 300–500ms periods of activity were randomly selected by the computer program and averaged together to get the estimated correlation for each cell. For reshuffling of spike times, only spikes occurring within the first 800ms of the UP state were randomly redistributed, and the minimum intercell spike interval was recalculated.

Using paired recordings, monosynaptic connections were detected by evoking single action potentials (at .1 Hz) in postsynaptic neurons (for excitatory connections) or by examining the latency, amplitude, rise time, and failure rate of recorded evoked IPSCs (for inhibitory connections). These values were recorded at 0 mV with a chloride reversal potential of −70 mV. For PC to PC pairs, single action potentials were similarly evoked, with the resulting EPSC recorded in the postsynaptic cell at −70 mV. 25 trials were subsequently averaged for each connected pair.

Analysis of IPSCs and EPSCs was performed using event detector programs (Synaptosoft, Inc www.synaptosoft.com). The amplitude of the events had to exceed a detection threshold set at the maximum limit of the noise (usually < 8pA). Rise times were measured from 10 to 90% of peak amplitude.

Statistics were implemented using InStat (GraphPad, La Jolla, CA). Briefly, a students' t-test was implemented for all comparisons, unless the distributions failed a normality test, in which case a Mann-Whitney was employed. In cases where there was a comparison of 2 or more datasets, a one-way ANOVA was used, and if the data could not be assumed to be sampled from Gaussian distributions, a Kruskal-Wallis was employed. For bin-by-bin comparisons of more than 2 samples, a repeated measures ANOVA was employed unless the data did not follow a Gaussian distribution in which case a Friedman test was used. Unless otherwise noted, all measurements are expressed as mean ± SEM.

## Results

Experiments were conducted in G42 and GIN GAD67- GFP transgenic mouse lines, in which PV positive and SOM positive neurons, respectively, are labeled with GFP throughout the cortex (Chattopadhyaya, 2004; Oliva et al., 2000). Although together these two populations are thought to represent the vast majority of the neocortical interneurons (Rudy et al., 2011; Xu et al., 2010), it is important to note that, in each of these mouse lines, only a subset of these population of neurons are labeled with GFP. We have previously

HHMI Author Manuscript HHMI Author Manuscript HHMI Author Manuscript

shown that GFP positive cells in layer 2/3 of the GIN mouse line are a relatively homogeneous population of Martinotti cells (Fino and Yuste, 2011b), but PV cells are more diverse, including basket cells, and chandelier cells, among others (Kozloski et al., 2001; Markram et al., 2004; Woodruff et al., 2009). Furthermore, in visual cortex (V1) of young G42 mice some GFP cells are PV negative (Buchanan et al., 2012).

In order to characterize the identity of GFP labeled neurons in somatosensory cortex (S1) of G42 mice we immunostained GFP positive cells for PV. In layer 2/3, we found good concordance between GFP and PV staining (Fig 1A; 91.2 ± 3.4 % of cells that were GFP positive were PV positive; n = 3 animals), similar to results reported in mature animals (Chattopadhyaya, 2004). Interestingly, in layers 4 and 5 this concordance dropped significantly (Fig. 1A2-3 and B,, layer 4: 71.5 ± 5.8 %, layer 5: 73.4 ± 6.5 %; n = 3 animals, $p < 0.01$ one-way ANOVA, L4 vs L5 $p > 0.05$, L2/3 vs L4 and L2/3 vs L5 $p < 0.01$ Tukey-Kramer multiple comparisons test). Finally, the percentage of GFP positive cells out of all labeled PV cells (or sparseness of the labeling) differed by layer, and was significantly smaller in layer 4 than either layers 2/3 or 5 (Fig. 1C; 39.6 ± 4.1% in L4 vs. 83.2 ± 6.8% in L2/3 and 78.4 ± 7.3 % L5, n = 3 animals, $p < 0.001$ one way ANOVA; L2/3 vs L4 and L4 vs L5 $p < 0.001$; L2/3 vs L5 $p > 0.05$ Tukey-Kramer multiple comparisons test). Since the co-localization of GFP and PV increases (and the sparseness of labeling decreases) throughout development, it is likely that PV expression matures with age and that the GFP positive, PV negative interneurons will eventually express PV (Buchanan et al., 2012; Chattopadhyaya, 2004). We refer to all GFP positive neurons in the SOM and PV GAD67 mouse lines as ‘sGFP’ and ‘pvGFP’ respectively, whereas unlabeled cells are referred to as ‘GFPneg’.

## Fast imaging of thalamically evoked activity in interneuron subtypes

To characterize the synchronous activity of sGFP, pvGFP and GFPneg neurons, we used thalamocortical somatosensory slices. These slices were bulk loaded with fura-2 AM (Fig. 2A), enabling two photon calcium imaging of action potential activity of neuronal populations in layers 2/3 and 4. A spatial light modulator (SLM) was used to split the two photon laser into multiple beamlets, and 40–50 neuron cell bodies within a 300 × 350 μm field of view within layers 2/3 and 4 of the barrel were targeted for fast imaging (Nikolenko et al., 2008) (Fig. 2B). The SLM obviated the need for raster scanning the laser, allowing us to take advantage of the spatial resolution and high signal to noise ratio two photon imaging affords, while collecting fluorescence at frame rates of 60–66 Hz with an Electron Multiplying CCD Camera (EMCCD).

We previously explored the effect of different frequencies of thalamic stimuli on cortical activity and found that high frequency (>10 Hz) stimulation was necessary to cause detectable activation in barrel cortex, whereas single stimuli failed to activate large numbers of cortical ensembles (MacLean et al., 2005). As before (MacLean et al., 2005), brief trains of six stimuli at 40 Hz, applied to the ventrobasal (VB) thalamus reliably activated groups of neurons (UP states) in both layers 2/3 and 4 (Fig. 2C). A fast nonnegative deconvolution filter was used to infer the most likely spike train of each neuron given the fluorescence observations (Vogelstein et al., 2010). To empirically adjust the parameters for the algorithm, we performed cell-attached patch clamp recordings from neurons identified during the stimulus driven cortical response. Because GFP expressing interneurons, particularly PV positive cells, may have different calcium buffering capacities, calibration was done in GFPneg, pvGFP, andsGFP cells (Fig. 2D). For all three cell types, the algorithm performed well at estimating the likelihood of a spike in any given frame, even when we made no allowance for a window of jitter around the time of the actual spike (Fig. 2E, GFPneg: sensitivity, 80.0 ± 2.5%, specificity, 98.1 ± 0.5% n = 11; pvGFP: sensitivity 78.0% ± 3.4% specificity 98% ± 0.8% n = 4, sGFP: sensitivity 82 ± 3.1% specificity 97.9 ± 0.6% n = 5), and detected nearly all spikes within a window of +/− 1 frame (GFPneg: sensitivity

HHMI Author Manuscript HHMI Author Manuscript HHMI Author Manuscript

95.0 ± 3.1%, specificity, 95.5 ± 1.4%, pvGFP: sensitivity 94 ± 4.1% specificity 96 ± 0.7%, sGFP: sensitivity 98.0 ± 2.9% specificity 94.3 ± 0.6% ). With the ability to detect single spikes with such high temporal resolution, we could address the timing of coordinated activity in subgroups of neurons at fast time scales.

## Activity of neocortical interneuron subtypes is not correlated

We first performed SLM imaging of pvGFP and sGFP GABAergic interneurons to study the timing of activity in these interneurons compared to other cell types. After stimulation of the thalamus, 35–75% of neocortical neurons were "active," or displayed at least a single 5% change in fluorescence, normalized to baseline ($\Delta F/F$), during thalamically triggered UP states. We typically imaged 5–15 pvGFP or sGFP interneurons alongside 20–40 GFPneg neurons (Fig. 3A). In both the G42 and GIN transgenic mouse lines, close to than 90% of GFPneg cells were excitatory as determined by their intrinsic electrophysiological properties (see below and (Gonchar et al., 2007; Peters, 1984), so we equate GFPneg with excitatory neurons. The probability of calcium activation of pvGFP cells, sGFP cells and GFPneg was found to be similar, with no significant differences between these cell types (Fig. 3B–C; pvGFP, 53.7 ± 5.4%; sGFP, 68.2 ± 4.6%; GFPneg, 56.4 ± 3.3%; one way ANOVA, p = . 08).

In order to address whether GABAergic interneurons subpopulations display more correlated firing than other cell types, we computed correlations from the deconvolved spike time estimates, which avoids overestimating the correlation coefficient that results from computing correlations directly from the raw fluorescence traces (Smith and Hausser, 2010). We first calculated these correlation coefficients among all pairs of active pvGFP, sGFP, or GFPneg cells during thalamically stimulated UP states. The normalized distributions of the correlations between pvGFP, sGFP and GFPneg cell pairs were similar, showing no significant differences when compared in a bin-by-bin manner (Fig. 3D; Friedman test, p = . 2874). While some cell pairs belonging to all cell types showed highly correlated activity (correlation coefficients greater than 0.6), in general all groups showed low correlations, with no significant difference between them (correlation among pvGFP neurons, 0.14 ± 0.01, n = 196 pairs; correlation among sGFP, 0.10 ± .01, n = 67 pairs; correlation among GFPneg cells, 0.12 ± .002, n = 3,119 pairs, from both G42 and GIN animals; p = .4198, Kruskal-Wallis test). Therefore, even when two cells belonged to the same cell class, they did not show similarities in firing when compared to other cell types.

We wondered whether there would be a significant inverse relationship between distance separating cell bodies and their activity correlations. In order to test this, we plotted the distance between cell bodies (in μm) vs. correlation coefficient for all cell pairs. We found, for all three groups, pvGFP, sGFP, and GFPneg no significant relationship between these two variables (Fig. 3E; pvGFP Pearson's R = −0.078, p = 0.27; sGFP Pearson's R = 0.0078, p =0.78; GFPneg Pearson's R = 0.019, p = 0.27). Therefore, neighboring neurons, even those of the same molecular subtype, do not have more correlated activity than those at further distances.

## Spiking synchrony of interneurons is similar to that of principal cells

Although using calcium imaging we found that PV or SOM interneurons did not show correlated activity, we could not exclude the possibility that these neurons were significantly correlated on a time scale faster than the temporal resolution of our SLM imaging (15ms). This seemed likely since interneurons belonging to both these subtypes have been shown to be coupled either chemically, and/or electrically via gap junctions, both of which can promote fast synchrony under certain conditions (Beierlein et al., 2000; Galarreta and Hestrin, 2001; Hu et al., 2011).

HHMI Author Manuscript HHMI Author Manuscript HHMI Author Manuscript

To examine this, we performed whole-cell electrophysiological recordings from 43 pvGFP interneurons in layer 2/3, with biocytin in our internal solution, and performed anatomical and electrophysiological analysis of these cells. Anatomically, pvGFP cells resembled basket cells, with densely branching axons, which have been shown to contact the perisomatic regions of postsynaptic targets (Fig. 4A, top). Physiologically, all of these cells were fast spiking interneurons, easily identified by their narrow spike width and large after hyperpolarization potentials (AHPs). In addition, these cells had high rheobases and fired at high frequencies in response to current injection (see Table 1, and Fig. 3A, bottom).

We also performed whole-cell electrophysiological recordings from 50 sGFP interneurons. All recorded cells were indeed interneurons, and were characterized both anatomically and physiologically, in a similar manner as pvGFP cells. Anatomically, sGFP cells had typically ascending axon collaterals that branched extensively in layer 1, characteristic of Martinotti cells (Fino and Yuste, 2011a; McGarry et al., 2010; Wang et al., 2004) (Fig. 4B, top). Electrophysiologically, in response to current injections, these cells displayed a lower rheobase than fast spiking cells, and a more moderate frequency of discharge, with significant spike frequency adaptation (see Table 1, and Fig. 4B, bottom). A vast majority of GFPneg cells (62/70 neurons) were confirmed, with a combination of intracellular recordings and anatomical reconstructions, to be excitatory pyramidal and regular spiking neurons, which will refer to as principal cells (“PCs” for the rest of this study, Fig. 4C).

To address the question of whether nearby interneurons have synchronous firing patterns, we patched pairs of interneurons within 100μm of each other in somatosensory cortex layer 2/3, where the probability of both chemical and electrical junctions between these cells is high (Galarreta and Hestrin, 2002). We patched 2–4 cells simultaneously to increase the likelihood of observing pairs in which at least 2 interneurons fired action potentials in response to thalamic stimulation (Fig. 5A). In addition, since we could record continuously for long periods of time, we were able to record spontaneously occurring UP states. For both thalamically evoked and spontaneously occurring activity, we calculated the time between spikes in every pair of two active cells. In this way, for each spike, we calculated the shortest time between spikes (“minimum inter-cell spike interval”) for the two cells patched (Fig. 5B). We performed this same analysis for pairs of excitatory PCs firing action potentials in response to thalamic stimulation. After extracting all minimum inter-cell spike intervals between all pairs of either pvGFP/pvGFP (n = 10 pairs) or sGFP/sGFP (n = 8 pairs) cells or PC/PC cells (n = 15 pairs, Fig. 5C), we constructed probability distributions of minimum time between spikes, which show the likelihood of a minimum inter-cell spike interval falling within any given 20 ms time bin, from 0 to 1 second. In performing this analysis, we limited our data set to experiments in which both neurons fired action potentials in at least 3 trials (cases in which both neurons did not spike in the same UP state were excluded from the analysis). Surprisingly, the overall minimum spike interval probability distributions were not statistically different between pvGFP, sGFP and PC cells when compared in a bin-by-bin manner (Fig. 5D, Friedman test, p = .6174,). This means that spikes do not occur more synchronously in these two interneuron populations than the general population of principal excitatory cells. We also calculated the average minimum time between spikes in all three cell types, and found no significant differences (pvGFP, 225 ± 18.8 ms, n = 12 pairs; sGFP, 191 ± 15.5 ms, n = 11 pairs; PC, 194 ± 9.93 ms, n = 18 pairs; p = 0.12, Kruskal-Wallis test,). Similarly, for spontaneously occurring activity, we found no difference in either the distribution of minimum spike times (Fig. 5E, p = .25, Friedman test), or the average minimum spike times (pvGFP, 209 ± 17.2 ms, n = 16; sGFP, 233 ± 16.1 ms, n = 6; PC, 191 ± 21 ms, n = 13, p = 0.08, Kruskal-Wallis test). In order to determine whether or not spiking was more or less synchronous than what would be expected by chance, we reshuffled the spikes, and recalculated the minimum interspike intervals. In all three cells types, PV, SOM and PC we found no differences in the average minimum spike

HHMI Author Manuscript HHMI Author Manuscript HHMI Author Manuscript

time intervals between the experimentally acquired data, and the randomly reshuffled data sets (PV, 247.7 ± 19.2 ms, p = .33; SOM, 200.6 ± 14.6 ms, p = 0.12; PC, 200.6 ± 10.0 ms, p = 0.51, in all cases Friedman test was used and reshuffled distributions were compared to evoked).

We next limited our analysis to pairs of interneurons coupled electrically. Interneurons were patched within 50–100 μm of one another, as shown in figure 6A. To measure electrical coupling, 500ms current steps were injected into one neuron or the other, and the coupling coefficient (CC) was defined as the ratio of the voltage deflection in the non-injected cell to the voltage deflection in the injected cell just before current offset, averaged over 10 sweeps and then averaged in the two directions of connectivity (Fig. 6B). Five out of the 12 pvGFP and 4 out of the 11 sGFP pairs were electrically coupled, with coupling coefficients of .031 ± .008 and .085 ± .012, respectively. UP states were then triggered with thalamic stimulation, and minimum inter-cell spike intervals were calculated. We found that the average inter-cell spike interval of electrically coupled pvGFP cells did not differ from uncoupled ones (Fig. 6D1 left column; 251.7 ± 52.4 ms, coupled vs 225 ± 18.8 ms, uncoupled p = 0.29, Mann-Whitney test). Similarly, for sGFP cell pairs, the average minimum intercell spike intervals was also not significantly different (Fig. 6D2 right column 183.2 ± 19.3ms, coupled vs 191 ± 15.5 ms, uncoupledp = .38, Mann-Whitney test).

Because many changes in plasticity and inhibition occur throughout development, we carried out a set of control experiments in young adult (p28-35) animals. Again, we observed no difference when we compared average minimum inter-cell spike intervals in coupled (n = 3) vs. uncoupled (n = 4) pvGFP cell pairs (Fig 6D2, left column, 221 ± 25.4ms coupled vs 238 ± 38.2 uncoupled, p = 0.41, Mann-Whitney test). This was also the case for electrically coupled (n =3) vs. uncoupled sGFP pairs (n = 5) (Fig. 6D2, right column, 214 ± 29.1 coupled vs 224 ± 18.5ms uncoupled, p = 0.37, Mann-Whitney test).

In the experiments outlined above, the slice exhibited spontaneous UP states, but at low frequencies (.005Hz ± .002Hz). We wondered whether our results were biased by the sparseness of activity, and sought to increase the frequency of the UP states so it would more closely resemble the slow oscillations seen in vivo (Hasenstaub et al., 2005; Luczak et al., 2007; Sanchez-Vives and McCormick, 2000). When slices were bathed in a modified version of ACSF with an increased Ca2+/Mg2+ ratio (Sanchez-Vives and McCormick, 2000; Xu et al., 2013) and 3.5mM potassium (‘normal $K^+$’), the frequency of the UP states increased significantly (Fig. 7A, top trace 0.047 ± .009 Hz, n =13; p<0.001, t-test). When we increased the potassium concentration to 5mM (‘high’ K+), we found that the frequency of the spontaneously occurring UP states increased even further (Fig 7A, bottom trace and Fig. 7B, 0.49 ± 0.04 Hz, n =5; p<0.001, t-test). We then calculated the duration of the UP states, and number of APs fired by each neuron during the UP state, and tested what effect thalamic stimulation would have under such conditions. We found that duration of each spontaneous UP state (‘spont’) was significantly longer in normal $K^+$ (3.33 ± 0.14 s) vs. high $K^+$ (1.36 ± 0.19 s). The duration of thalamically stimulated UP states (‘stim’) was also significantly longer in normal K+ vs. high $K^+$ (3.02 ± 0.18 s vs 1.53 ± 0.24s), and these durations did not differ significantly from spontaneous in each condition (Fig. 7C; p < 0.001, one-way ANOVA; p < .001 ‘normal K+’ vs ‘high K+’ spont and ‘normal K+’ vs ‘high K+’ stim, p > .05 ‘spont’ vs ‘stim’ normal K+ and ‘spont’ vs ‘stim’ high K+, Tukey-Kramer multiple comparisons test). The number of action potentials fired by each neuron was on average significantly higher in normal K+ (3.05 ± 0.24) vs. high K+ (1.84 ± 0.39). Likewise, the number of action potentials fired during thalamically stimulated UP states was significantly higher in normal K+ (3.59 ± 0.27) vs. high K+ (2.05 ± 0.63), but again these values did not differ significantly from spontaneous UP states in either K+ concentration (Fig. 7D; p < 0.001, one-way ANOVA; p < 0.01 ‘normal K+’ vs ‘high K+’ spont and ‘normal K+’ vs

HHMI Author Manuscript HHMI Author Manuscript HHMI Author Manuscript

'high K+' stim, $p > 0.05$ 'spont' vs 'stim' normal K+ and 'spont' vs 'stim' high K+, Tukey-Kramer multiple comparisons test). These results are in good agreement with previous work showing that thalamically evoked and spontaneous occurring UP states activate the same sub-networks in cortex (Luczak et al., 2007; MacLean et al., 2005). We now extend this work, showing that even in an oscillating preparation with UP states that occur more frequently but are shorter in duration, thalamic stimulation evokes activations that retain the properties of spontaneous activity. Using this preparation with higher frequencies of UP states, we investigated whether interneurons would be more or less synchronous than PCs. We again calculated the minimum inter-cell spike interval among PV cells and PCs within 100μm of one another, and plotted the distributions for both spontaneous and thalamically triggered UP states. For both spontaneously occurring and stimulated UP states, we found no difference in mean minimum interspike interval for PV (168.1 ± 16.4ms spont; 172.9 ± 19.7 stim, n = 5 pairs) vs. PCs (179.8 ± 15.9 ms spont, 181.4 ± 14.5 n = 8 pairs) ($p = 0.32$ stim comparisons, $p = 0.52$ spont comparisons; Kruskal-Wallis test). A similar result was found when comparing the probability distributions of minimum interspike intervals in a bin by bin fashion (Fig. 7E–F $p = 0.27$ spont, $p = 0.33$ stim, Friedman test). Therefore, at least under the various parameters we tested, electrical coupling does not significantly alter synchronous firing in interneurons.

## IPSCs, but not EPSCs, show high correlation during spontaneous and thalamically-evoked cortical activations

Since we found, in both our imaging and electrophysiological studies, that interneurons do not exhibit strong synchrony during thalamically evoked or spontaneous activity, we next investigated the timing of inhibitory postsynaptic potentials (IPSCs), compared to excitatory postsynaptic potentials (EPSCs) in nearby PC cells. Such a measurement would be representative of all synaptic inputs and could lend insight into the functional organization of inhibition vs. excitation within individual cells. To this end, we used single-electrode voltage clamp to separate inhibitory postsynaptic potentials (IPSCs) from excitatory postsynaptic potentials (EPSCs). We used an intracellular solution with a chloride reversal of −70mV, allowing us to isolate EPSCs at this potential, while IPSCs were isolated by clamping at 0mV (Fig. 8A). Two to four PC cells within 200 μm within the same layer (2/3) and barrel were patch clamped, and EPSCs and IPSCs were recorded from these cells on alternate trials, during both triggered and spontaneous activations.

We found that IPSCs showed significantly higher correlations than EPSCs in both thalamically-triggered (Figs. 8B–C, EPSCs .55 ± .04; IPSCs, R = .76 ± .04, n = 43 pairs; $p < 0.001$, Mann-Whitney test, n = 43 pairs) and spontaneous cortical activity (EPSCs .46 ± .04, IPSCs, R = .66 ± .04 n = 26 pairs; $p < 0.01$, Mann-Whitney test). Analysis of the cross correlation of EPSCs and IPSCs revealed the half width at half height of the cross correlogram was significantly wider for EPSCs than IPSCs, (Fig. 8D 156.2 ± 17.1 ms for EPSCs; 68.2 ± 7.49 ms for IPSCs; $p < 0.001$, Mann-Whitney Test).

Because IPSCs and EPSCs during UP states have very different rise times (IPSC 3.67 ± 0.24 ms, EPSC 2.14 ± 0.17; $p < 0.001$; n = 27 cells, unpaired t test with Welch correction), decay times (IPSC 17.50 ± 1.90ms, EPSC 8.85 ± 0.45ms; $p < 0.001$; n = 27 cells), and amplitudes (IPSC 77.14 ± 8.80 pA, EPSC 22.16 ± 1.51 pA; $p < 0.001$), it is possible that these parameters could affect the values of correlation obtained by correlating the raw traces. More specifically, the longer decay times typically seen in IPSCs could increase the correlation value. To address this issue, we detected the times of peaks of both EPSCs and IPSCs, converted these into binary time vectors, and correlated these vectors, using time bins of three different sizes (1, 10, and 100 milliseconds). In this way, instead of correlating the events themselves, we correlated only the timing of the events. But even at the smallest time bins analyzed (1ms), the time vectors of IPSCs were significantly more correlated than

HHMI Author Manuscript HHMI Author Manuscript HHMI Author Manuscript

EPSC time vectors (Fig. 9A; EPSCs, R = .037 ± .02; IPSCs, R = .090 ± 0.01 .p < 0.001, unpaired t-test, n = 27 pairs). This was also true at larger time bins we checked, 10ms (Fig. 9B; EPSCs, R = .181 ± .02; IPSCs, R = .454 ± .01; unpaired t test, p < 0.001), and 100ms (Fig. 9C; EPSCs, R = .360 ± .025; IPSCs, R = .695 ± .027; unpaired t-test, p < 0.001), in both spontaneously occurring and triggered cortical activity. These results indicated that inhibitory potentials are significantly more correlated than excitatory ones, a finding apparently at odds with our previously found lack of difference in the correlation of firing of excitatory and inhibitory cells.

## Common inhibitory input underlies correlated IPSCs

Two different scenarios could explain the synchronous IPSCs we found during triggered and spontaneous activity. First, it is possible that interneurons are firing more synchronously than their excitatory counterparts, and such synchronization would lead to IPSCs occurring at the same time in nearby pyramidal cells (Fig. 10A, left). Although this could explain the high degree of IPSC correlations observed, our population imaging and dual intracellular recordings failed to show any significant difference in the correlations between pyramidal cells and interneurons. A second possibility is that the higher correlation of IPSCs could be due to shared presynaptic input, emanating from the same neuron. In this case, an interneuron would have to be densely connected to downstream pyramidal cells within the distances we tested (30–200 μm). If this were true, each time an inhibitory interneuron fired an action potential, it would generate a synchronous IPSC in its downstream targets, thus explaining the emergence of correlated IPSCs (Fig. 10A, right).

Since our imaging and electrophysiological experiments led us to conclude that only a minority of the high correlation we observed in IPSCs could be due to synchronous firing, we hypothesized that a high degree of overlapping input from nearby interneurons was primarily responsible for the correlated IPSCs. If correlation of IPSCs is due to shared input rather than synchronous firing, two criteria would need to be met: 1) inhibitory connections onto PCs should be much more dense locally than connections from PCs to PCs and 2) each IPSC detected during the thalamic response should be attributable to just one or a few interneurons. In order to investigate this, we performed paired recordings between either pvGFP cells and PCs, or SOM cells and PCs. We found that, within 150 μm, 79.8 ± 12.0% of dually patched pvGFP and PC cell pairs were monosynaptically connected. We found a similarly high connection probability between sGFP cells and PC cell pairs (74.8 ± 11.0%) whereas the connection probability between PC pairs was significantly lower 9.8 ± 3.1%; (Fig. 10B $p = 0.001$, Kruskal Wallis; $p < 0.01$ for PC vs pvGFP and PC vs sGFP; $p > 0.05$ for pvGFP vs sGFP, Dunn's multiple-comparison test). This high probability of connection of interneurons onto PCs fulfills the first criteria, and is consistent with recent results demonstrating a dense connectivity from somatostatin and parvalbumin positive interneurons to neighboring pyramidal cells (Fino and Yuste, 2011a; Packer and Yuste, 2011). We also examined how correlations of IPSCs and EPSCs drop off with distance, since connection probability of both PV→PC and SOM→ PC has been shown to drop off steeply with distance (Fino and Yuste, 2011a; Packer and Yuste, 2011). Our rationale was that if synchronization was causing the high correlations of IPSCs, the correlations we observed may remain higher over larger distances than would be expected if they were caused by common input. In accordance with this, both IPSCs and EPSCs dropped off rapidly with distance, with slopes significantly different from zero (Fig 10C EPSCs, n = 30 pairs, $r_{corr} = -0.67$, p < 0.001; IPSCs, n = 25 pairs, R = −0.72 p < 0.001; linear regression) with no difference in their slopes (analysis of covariance p = 0.52).

Next, in order to estimate of how many interneurons contribute to each IPSC during cortical activity, we measured the conductance of IPSCs during triggered activity, and compared these to the conductance of monosynaptic pvGFP→PC and sGFP→PC IPSCs, as measured

HHMI Author Manuscript HHMI Author Manuscript HHMI Author Manuscript

from paired recordings. The mean conductance of pvGFP→PC connections was significantly higher than that of sGFP→PC connections (pvGFP→PC, 2.08 ± 0.50 nS; sGFP→PC, 0.76 ± 0.24 nS, t test, $p < .05$, n = 10 for pGFP→PC pairs and n = 15 sGFP→PC pairs), which is unsurprising given our recordings were made at the soma, much nearer to where parvalbumin interneurons form synapses onto PCs. More importantly, the mean conductances during cortical activity (1.11 ± 0.02 nS, n = 6578 IPSCS recorded from 15 cells) did not differ significantly from the average conductances of monosynaptic, single axon, PV and SOM inputs (1.38 ± 0.29 nS; p = 0.442, Mann-Whitney, n = 25, normalized distributions shown in Fig. 10D). In addition, the failure rate of IPSCs was extremely low (nearly 0%, data not shown), which would ensure that given a dense connectivity scheme, as each time an interneuron fired an action potential it would be recorded in all its downstream targets. Finally, as illustrated in Table 2, the rise time, decay, amplitude and half-width of IPSCs measured from paired recordings did not significantly differ from IPSCs recorded during UP states ($p < 0.001$ for all comparisons, student's t-test). This indicates that each IPSC observed during triggered or spontaneous activity could be generated by just one or at most a few interneurons, fulfilling the second criteria discussed above. We conclude that high correlation of IPSCs seen during thalamically driven UP states must be primarily due to shared presynaptic input from inhibitory neurons rather than synchronous firing of interneurons.

## Decreasing inhibition correlates neural activity

With inhibition itself being asynchronous, we wondered whether a functional role of inhibition could be to *desynchronize,* rather than synchronize, the local network. In fact, several network models have proposed that a dynamic balance of excitatory and inhibitory fluctuations counteracts correlations induced by common inputs (Hertz, 2010; Renart et al., 2010). However, direct experimental evidence in support of these models has been scant. In their theoretical model of decorrelated networks, Renart et al proposed that while isolated EPSCs and IPSCs can be correlated due to common input, these correlations cancel one another, and therefore fall off at intermediate membrane potentials. To test the validity of this model, we again patched 2–4 neurons within 100μm of one another in voltage clamp during thalamic UP states. We then recorded correlations in membrane potential at several voltages from −70 to 0mV (Fig. 11A). Interestingly, our experimental data was similar to what was predicted by the model in that the correlation coefficients were highest at the extremes of voltages (−70mV and 0mV, Figure 11B*,* n = 18 pairs), where either mostly EPSCs or IPSCs, respectively, were recorded. Importantly, at intermediate voltages (n = 8 pairs), the correlation coefficient drops off. This is attributed to the fact that when EPSCs and IPSCs are themselves correlated, as is the case during both spontaneous and sensory evoked activity in somatosensory cortex (Okun and Lampl, 2008) the correlations in EPSCs and IPSCs occur simultaneously and cancel, leading to a significant reduction in the correlation of membrane potential. A natural consequence of this is that the correlation of output spikes in this scenario will also be low, as we have shown here is the case during UP states.

In a final set of experiments, we hypothesized that if indeed inhibitory currents decorrelated excitatory ones, reducing inhibitory currents should have the opposite effect, *increasing* membrane potential correlations. To test this, we reduced inhibition with nanomolar (100–200nm) amounts of gabazine (SR-95531), and reassessed the correlation coefficients of excitatory currents among two cells within 100μm of one another (Fig. 11*C*). At these concentrations of gabazine, while there is mild reduction of inhibitory currents, epilepsy is not observed (Sanchez-Vives et al., 2010). We found that the pairwise correlation coefficients of EPSCs significantly increased with 100nm gabazine in the bath, and further increased at 200nm of gabazine (Fig. 11D control, R = 0.31 ± 0.04,; 100nm gabazine, R=

HHMI Author Manuscript HHMI Author Manuscript HHMI Author Manuscript

0.58 ± 0.05; 200nm gabazine, R = 0.66 ± 0.05;p < 0.05 control vs 100nm and control vs 200nm Mann-Whitney, n = 5 pairs). Since disinhibition increases firing rates which may spuriously increase correlations, we sought to determine what effect blocking inhibition had on correlations of reshuffled data. The correlations of reshuffled data did not differ significantly in either 100nm or 200nm of the drug (control, R = 0.04 ± .02; 100nm, 100nm GZ, R = 0.07 ± 0.03; 200nm GZ, R = 0.16 ± 0.05 p = 0.90 for control vs. 100nm, p = 0.34 for control vs. 200nm, n = 5 pairs). We therefore conclude that there is a causal link between the presence of inhibition and the decorrelated firing of excitatory cells, and that interneurons may be acting to decrease rather than increase correlated activity.

## Discussion

We used fast, two-photon calcium imaging and electrophysiology to study the correlations in neuronal spiking activity within three major subclasses: PV and SOM expressing interneurons, and pyramidal cells. Interneurons exhibited low correlations in response to both thalamic stimulation and during spontaneously occurring UP states. This uncorrelated activity was a general feature of all neurons; even interneurons within a subclass did not exhibit correlated firing when compared to pyramidal cells. Intracellular recordings confirmed that the distribution of minimum inter-cell spike intervals was not significantly different among interneuronal subtypes and/or excitatory cells. Surprisingly, even cell pairs connected by gap junctions did not display tight synchrony as previously reported (Deans et al., 2001; Di Garbo et al., 2005; Galarreta and Hestrin, 2001; Tamas et al., 2000). On the other hand, in apparent contradiction with these findings, voltage clamp recordings demonstrated IPSCs *are* indeed correlated in cells at close distances, but we found that this phenomenon is due mostly to shared input rather than synchronous firing. Our data thus indicate that, during cortical UP states, asynchronous activity is a general feature of all cortical cells, regardless of cell class. Since UP states represent recurrent activity within local circuits we propose that this uncorrelated activity may serve to provide a backdrop upon which sensory discriminations can be more easily be decoded (Abbott and Dayan, 1999).

### Cortical interneurons have uncorrelated firing during UP states

While it is clear that there are many subtypes of GABAergic interneurons (Ascoli et al., 2008), we know little about whether different subtypes respond differently to stimuli. Improvements in the ability to identify interneurons has allowed for the assessment of correlations among these cells during sensory driven and spontaneous behavior (Hofer et al., 2011). While this study was highly informative, the authors addressed the issue of synchrony at a time scale of hundreds of milliseconds, which has fundamentally different consequences on information processing. Our findings, using high speed imaging, demonstrate that subtype specificity does not confer correlated spiking activity in response to thalamically driven or spontaneously occurring UP states. In addition, we find that nearby neurons do not have more correlated activity than those at further distances, at least within the relatively close distances examined.

A drawback of our imaging experiments is that, although PV and SOM neurons were selectively labeled, there are many further subdivisions that can be made. PV interneurons, especially, are thought to represent a number of subtypes including, but not limited to, basket cells, chandelier cells and multipolar bursting (MB) interneurons (Blatow et al., 2003; Wang et al., 2004). Likewise, SOM cells belong to at least 3 distinct subclasses (McGarry et al., 2010). Therefore one possible interpretation of our imaging data is that it simply did not afford the resolution necessary to detect synchrony among interneurons of the same subclass, within the PV and SOM labeled subtypes.

HHMI Author Manuscript HHMI Author Manuscript HHMI Author Manuscript

Our data showing uncorrelated activity among interneurons is surprising given that interneurons are often coupled both electrically and synaptically, and that such coupling can promote synchrony under certain conditions (Galarreta and Hestrin, 2001; Hu et al., 2011). In these studies spiking was induced by introducing current injections in both cells simultaneously, or by activating specific subsets of neurons using neuromodulators. These manipulations do not activate all the conductances relevant during evoked or spontaneous activity in sensory cortex. The interaction of these conductances, combined with the electrical and chemical coupling of interneurons, is important when testing whether this coupling affects synchrony; when neurons are in a high conductance state, as we and others have found is the case during UP states (Bruno and Sakmann, 2006; Gonzalez-Burgos and Barrionuevo, 2001; Watson et al., 2008) (with one exception (Waters and Helmchen, 2006)), it is possible that gap junction and inhibitory synaptic coupling have a much smaller functional effect. The main role of gap junctions may be to act as low pass filters, synchronizing subthreshold membrane potentials, and promoting synchrony over broader time scales (Galarreta and Hestrin, 1999, 2001). Alternatively, gap junctions could play a metabolic or developmental role, by enabling cells that belong to the same differentiation program to share second messengers or signaling molecules (Yuste et al., 1992).

Another important limitation of our work is that it was carried out in an acute slice preparation, where connections are severed, and there is no neuromodulation. Although the in vitro slice preparation is widely used to examine synaptic dynamics or plasticity and cellular studies, the question remains whether the slice preparation is appropriate for the examination of neuronal population dynamics. However, the network activity we studied here, matches well with that previously reported in large scale in vivo imaging studies of sensory cortices (Kenet et al., 2003; Petersen et al., 2003). More specifically, UP states have been widely reported in vivo where they are thought to occur in an oscillatory manner during slow wave sleep, quiet wakefulness, and under certain types of anesthesia (Luczak et al., 2007; Monier et al., 2003; Sanchez-Vives and McCormick, 2000; Steriade et al., 2001). In order to more closely mimic these oscillations, and to examine what effect they may have on interneuron synchrony, we used a modified ACSF with increased potassium, and found that even during UP states occurring under these conditions, interneurons were not synchronous. In addition, high frequency thalamic stimulation in these conditions evoked UP states closely resembling the spontaneously occurring ones, which has also been found to be the case *in vivo* (Luczak et al 2007). Regardless of the functional role of UP states, they are a well-established form of network activity that is preserved in slices, where they can be studied in a reduced model (MacLean et al., 2005; Poulet and Petersen, 2008; Watson et al., 2008; Xu et al., 2013). Therefore, some of the same mechanisms underlying our main results are likely to be present in vivo, even if they do not represent the full spectrum of dynamics observed in awake behaving animals.

## Dense inhibitory connectivity leads to synchronous IPSCs

In the experiments performed here, we found that when we voltage clamped cells within 100μm at the reversal potentials for inhibition or excitation, isolated EPSCs and IPSCs were highly correlated, with IPSCs much more highly correlated than EPSCs. This result is similar to findings in ferret, where the higher degree of correlation among IPSCs in dually patched cells was attributed to synchronization of PV interneurons within the gamma band (Hasenstaub et al., 2005). However, several lines of evidence lead us to conclude the high correlation we observed in IPSCs is due to a greater degree of shared inhibitory inputs among nearby cells. First, inhibitory neurons, as discussed above, do not fire more synchronously than pyramidal cells. Second, the high probability of finding a connection between parvalbumin-positive and somatostatin-positive interneurons onto pyramidal cells, indicates that shared inhibitory input is likely the main mechanism responsible for IPSC

HHMI Author Manuscript HHMI Author Manuscript HHMI Author Manuscript

correlation we observed. This finding is in agreement with previous electrophysiological and two photon mapping studies demonstrating both SOM and PV interneuron subtypes make locally dense and unspecific connections (Fino and Yuste, 2011a; Packer and Yuste, 2011). In fact when we calculated the decay constant over which the probability of PV→ PC connections tapered off (166.8μm; (Packer and Yuste, 2011)) we found it agreed well with the decay constant over which correlations tapered off (165.5μm, see Fig. 9). Finally, the conductance of each IPSC detected during spontaneous and evoked activity was comparable to the conductance of individual synapses, indicating that the IPSCs during evoked and spontaneous activity could be comprised of just a single interneuron firing, rather than a synchronous group.

### Inhibition as a decorrelator of neuronal circuits

The extent of membrane potential and/or spiking correlations among nearby neurons or those sharing receptive fields varies greatly across studies, in part due the manner in which such correlations are calculated (Cohen and Kohn, 2011). In particular, low spike rates like those observed during cortical UP states tend to decrease correlations. For this reason, we used principal cells as a metric for evaluating the significance of synchrony among inhibitory subtypes, and found that correlations among interneurons did not differ from principal cells. In order to evaluate whether or not the principal cells had significant correlated firing, we used reshuffling techniques, which demonstrated that these cells do not fire any more synchronously than what would be expected if their spikes were randomly distributed. We conclude that the firing of *both* inhibitory cells and principal cells during UP states is asynchronous.

Taken together, our findings are in good agreement with recent studies in mouse and monkey primary visual cortices showing that, even when neurons share receptive fields, they do not have high firing rate correlations. (Ecker et al., 2010; Hofer et al., 2011; Smith and Hausser, 2010). In both these studies, the authors speculated that their observations could be due to some unknown, active mechanism of decorrelation. Theoretical work has suggested this mechanism could be in part due to inhibitory inputs balancing excitatory ones, effectively canceling correlations (Renart et al., 2010). In this model when both inhibitory and excitatory inputs are correlated, inhibition closely follows excitation, thereby reducing the correlated fluctuations, and leading to sparse spiking. This may explain why the EPSC and IPSC correlations fell off with distance (Fig. 10C) while we saw no such relationship for neuronal activity (Fig. 3e). We propose that by *preventing* uncontrolled network-wide synchrony rather than promoting it, inhibition may create a background of weakly-correlated spiking, as required for efficient information processing based on either firing rates or coordinated spike timing patterns (Vogels and Abbott, 2009).

## Acknowledgments

We thank A. Packer and A. Woodruff, and T. Machado for helpful feedback on this work, Y. Shin for anatomical reconstructions, M. Karnani, A. Pala, and C. Petersen for reagents and technical assistance with immunohistochemistry, and members of the Yuste lab for help and comments. Supported by the Kavli Institute for Brain Science, NEI, NINDS, NIHM, NIDA, Keck Foundation and NARSAD. This material is based upon work supported by, or in part by, the U. S. Army Research Laboratory and the U. S. Army Research Office under contract number W911NF-12-1-0594.

## References

Abbott LF, Dayan P. The effect of correlated variability on the accuracy of a population code. Neural Comput. 1999; 11:91–101. [PubMed: 9950724]

Agmon A, Connors BW. Thalamocortical responses of mouse somatosensory (barrel) cortex in vitro. Neuroscience. 1991; 41:365–379. [PubMed: 1870696]

HHMI Author Manuscript HHMI Author Manuscript HHMI Author Manuscript

Ascoli GA, Alonso-Nanclares L, Anderson SA, Barrionuevo G, Benavides-Piccione R, Burkhalter A, Buzsaki G, Cauli B, Defelipe J, Fairen A, et al. Petilla terminology: nomenclature of features of GABAergic interneurons of the cerebral cortex. Nature reviews Neuroscience. 2008; 9:557–568.

Bartos M, Vida I, Frotscher M, Meyer A, Monyer H, Geiger JR, Jonas P. Fast synaptic inhibition promotes synchronized gamma oscillations in hippocampal interneuron networks. Proc Natl Acad Sci USA. 2002; 99:13222–13227. [PubMed: 12235359]

Beierlein M, Gibson JR, Connors BW. A network of electrically coupled interneurons drives synchronized inhibition in neocortex. Nat Neurosci. 2000; 3:904–910. [PubMed: 10966621]

Blatow M, Rozov A, Katona I, Hormuzdi SG, Meyer AH, Whittington MA, Caputi A, Monyer H. A novel network of multipolar bursting interneurons generates theta frequency oscillations in neocortex. Neuron. 2003; 38:805–817. [PubMed: 12797964]

Bruno RM. Synchrony in sensation. Current opinion in neurobiology. 2011; 21:701–708. [PubMed: 21723114]

Bruno RM, Sakmann B. Cortex is driven by weak but synchronously active thalamocortical synapses. Science. 2006; 312:1622–1627. [PubMed: 16778049]

Buchanan KA, Blackman AV, Moreau AW, Elgar D, Costa RP, Lalanne T, Tudor Jones AA, Oyrer J, Sjostrom PJ. Target-specific expression of presynaptic NMDA receptors in neocortical microcircuits. Neuron. 2012; 75:451–466. [PubMed: 22884329]

Chattopadhyaya B. Experience and Activity-Dependent Maturation of Perisomatic GABAergic Innervation in Primary Visual Cortex during a Postnatal Critical Period. Journal of Neuroscience. 2004; 24:9598–9611. [PubMed: 15509747]

Cohen MR, Kohn A. Measuring and interpreting neuronal correlations. Nat Neurosci. 2011; 14:811–819. [PubMed: 21709677]

Deans MR, Gibson JR, Sellitto C, Connors BW, Paul DL. Synchronous activity of inhibitory networks in neocortex requires electrical synapses containing connexin36. Neuron. 2001; 31:477–485. [PubMed: 11516403]

Di Garbo A, Panarese A, Chillemi S. Gap junctions promote synchronous activities in a network of inhibitory interneurons. Biosystems. 2005; 79:91–99. [PubMed: 15649593]

Ecker AS, Berens P, Keliris GA, Bethge M, Logothetis NK, Tolias AS. Decorrelated Neuronal Firing in Cortical Microcircuits. Science. 2010; 327:584–587. [PubMed: 20110506]

Feldmeyer D, Egger V, Lubke J, Sakmann B. Reliable synaptic connections between pairs of excitatory layer 4 neurones within a single 'barrel' of developing rat somatosensory cortex. J Physiol. 1999; 521(Pt 1):169–190. [PubMed: 10562343]

Ferster D, Lindstrom S. Synaptic excitation of neurones in area 17 of the cat by intracortical axon collaterals of cortico-geniculate cells. J Physiol. 1985; 367:233–252. [PubMed: 4057098]

Fino E, Yuste R. Dense Inhibitory Connectivity in Neocortex. Neuron. 2011a; 69:1188–1203. [PubMed: 21435562]

Fino E, Yuste R. Dense inhibitory connectivity in neocortex. Neuron. 2011b; 69:1188–1203. [PubMed: 21435562]

Galarreta M, Hestrin S. A network of fast-spiking cells in the neocortex connected by electrical synapses. Nature. 1999; 402:72–75. [PubMed: 10573418]

Galarreta M, Hestrin S. Spike transmission and synchrony detection in networks of GABAergic interneurons. Science. 2001; 292:2295–2299. [PubMed: 11423653]

Galarreta M, Hestrin S. Electrical and chemical synapses among parvalbumin fast-spiking GABAergic interneurons in adult mouse neocortex. Proc Natl Acad Sci U S A. 2002; 99:12438–12443. [PubMed: 12213962]

Gentet LJ, Avermann M, Matyas F, Staiger JF, Petersen CC. Membrane potential dynamics of GABAergic neurons in the barrel cortex of behaving mice. Neuron. 2010; 65:422–435. [PubMed: 20159454]

Gibson JR, Beierlein M, Connors BW. Two networks of electrically coupled inhibitory neurons in neocortex. Nature. 1999; 402:75–79. [PubMed: 10573419]

Gibson JR, Beierlein M, Connors BW. Functional properties of electrical synapses between inhibitory interneurons of neocortical layer 4. J Neurophysiol. 2005; 93:467–480. [PubMed: 15317837]

HHMI Author Manuscript HHMI Author Manuscript HHMI Author Manuscript

Gonchar Y, Wang Q, Burkhalter A. Multiple distinct subtypes of GABAergic neurons in mouse visual cortex identified by triple immunostaining. Front Neuroanat. 2007; 1:3. [PubMed: 18958197]

Gonzalez-Burgos G, Barrionuevo G. Voltage-gated sodium channels shape subthreshold EPSPs in layer 5 pyramidal neurons from rat prefrontal cortex. J Neurophysiol. 2001; 86:1671–1684. [PubMed: 11600631]

Gordon JA. Oscillations and hippocampal-prefrontal synchrony. Current opinion in neurobiology. 2011; 21:486–491. [PubMed: 21470846]

Hasenstaub A, Shu Y, Haider B, Kraushaar U, Duque A, McCormick DA. Inhibitory postsynaptic potentials carry synchronized frequency information in active cortical networks. Neuron. 2005; 47:423–435. [PubMed: 16055065]

Hertz J. Cross-correlations in high-conductance states of a model cortical network. Neural Comput. 2010; 22:427–447. [PubMed: 19842988]

Hofer SB, Ko H, Pichler B, Vogelstein J, Ros H, Zeng H, Lein E, Lesica NA, Mrsic-Flogel TD. Differential connectivity and response dynamics of excitatory and inhibitory neurons in visual cortex. Nature neuroscience. 2011; 14:1045–1052.

Hu H, Ma Y, Agmon A. Submillisecond firing synchrony between different subtypes of cortical interneurons connected chemically but not electrically. J Neurosci. 2011; 31:3351–3361. [PubMed: 21368047]

Kaminski J, Wrobel A, Kublik E. Gap junction blockade eliminates supralinear summation of fast (>200Hz) oscillatory components during sensory integration in the rat barrel cortex. Brain Res Bull. 2011

Kenet T, Bibitchkov D, Tsodyks M, Grinvald A, Arieli A. Spontaneously emerging cortical representations of visual attributes. Nature. 2003; 425:954–956. [PubMed: 14586468]

Kozloski J, Hamzei-Sichani F, Yuste R. Stereotyped position of local synaptic targets in neocortex. Science. 2001; 293:868–872. [PubMed: 11486089]

Luczak A, Bartho P, Marguet SL, Buzsaki G, Harris KD. Sequential structure of neocortical spontaneous activity in vivo. Proc Natl Acad Sci U S A. 2007; 104:347–352. [PubMed: 17185420]

MacLean JN, Watson BO, Aaron GB, Yuste R. Internal dynamics determine the cortical response to thalamic stimulation. Neuron. 2005; 48:811–823. [PubMed: 16337918]

Markram H, Toledo-Rodriguez M, Wang Y, Gupta A, Silberberg G, Wu C. Interneurons of the neocortical inhibitory system. Nature reviews Neuroscience. 2004; 5:793–807.

McClurkin JW, Optican LM, Richmond BJ, Gawne TJ. Concurrent processing and complexity of temporally encoded neuronal messages in visual perception. Science. 1991; 253:675–677. [PubMed: 1908118]

McGarry LM, Packer AM, Fino E, Nikolenko V, Sippy T, Yuste R. Quantitative classification of somatostatin-positive neocortical interneurons identifies three interneuron subtypes. Front Neural Circuits. 2010; 4:12. [PubMed: 20617186]

Monier C, Chavane F, Baudot P, Graham LJ, Fregnac Y. Orientation and direction selectivity of synaptic inputs in visual cortical neurons: a diversity of combinations produces spike tuning. Neuron. 2003; 37:663–680. [PubMed: 12597863]

Nikolenko V, Watson BO, Araya R, Woodruff A, Peterka DS, Yuste R. SLM Microscopy: Scanless Two-Photon Imaging and Photostimulation with Spatial Light Modulators. Front Neural Circuits. 2008; 2:1–14. [PubMed: 18946541]

Okun M, Lampl I. Instantaneous correlation of excitation and inhibition during ongoing and sensory-evoked activities. Nat Neurosci. 2008; 11:535–537. [PubMed: 18376400]

Oliva AA Jr, Jiang M, Lam T, Smith KL, Swann JW. Novel hippocampal interneuronal subtypes identified using transgenic mice that express green fluorescent protein in GABAergic interneurons. J Neurosci. 2000; 20:3354–3368. [PubMed: 10777798]

Packer AM, Yuste R. Dense, unspecific connectivity of neocortical parvalbumin-positive interneurons: a canonical microcircuit for inhibition? The Journal of neuroscience : the official journal of the Society for Neuroscience. 2011; 31:13260–13271. [PubMed: 21917809]

Peters, AJ.; EG, editors. Cellular Components of the Cerebral Cortex. New York: Plenium; 1984.

Petersen CC, Grinvald A, Sakmann B. Spatiotemporal dynamics of sensory responses in layer 2/3 of rat barrel cortex measured in vivo by voltage-sensitive dye imaging combined with whole-cell

HHMI Author Manuscript HHMI Author Manuscript HHMI Author Manuscript

voltage recordings and neuron reconstructions. J Neurosci. 2003; 23:1298–1309. [PubMed: 12598618]

Poulet JF, Petersen CC. Internal brain state regulates membrane potential synchrony in barrel cortex of behaving mice. Nature. 2008; 454:881–885. [PubMed: 18633351]

Renart A, de la Rocha J, Bartho P, Hollender L, Parga N, Reyes A, Harris KD. The Asynchronous State in Cortical Circuits. Science. 2010; 327:587–590. [PubMed: 20110507]

Rudy B, Fishell G, Lee S, Hjerling-Leffler J. Three groups of interneurons account for nearly 100% of neocortical GABAergic neurons. Dev Neurobiol. 2011; 71:45–61. [PubMed: 21154909]

Sanchez-Vives MV, Mattia M, Compte A, Perez-Zabalza M, Winograd M, Descalzo VF, Reig R. Inhibitory modulation of cortical up states. J Neurophysiol. 2010; 104:1314–1324. [PubMed: 20554835]

Sanchez-Vives MV, McCormick DA. Cellular and network mechanisms of rhythmic recurrent activity in neocortex. Nat Neurosci. 2000; 3:1027–1034. [PubMed: 11017176]

Sanes JN. Neocortical mechanisms in motor learning. Current opinion in neurobiology. 2003; 13:225–231. [PubMed: 12744978]

Smith SL, Häusser M. Parallel processing of visual space by neighboring neurons in mouse visual cortex. Nature Neuroscience. 2010; 13:1144–1149.

Steriade M, Timofeev I, Grenier F. Natural waking and sleep states: a view from inside neocortical neurons. J Neurophysiol. 2001; 85:1969–1985. [PubMed: 11353014]

Tamas G, Buhl EH, Lorincz A, Somogyi P. Proximally targeted GABAergic synapses and gap junctions synchronize cortical interneurons. Nat Neurosci. 2000; 3:366–371. [PubMed: 10725926]

Uhlhaas PJ, Roux F, Rodriguez E, Rotarska-Jagiela A, Singer W. Neural synchrony and the development of cortical networks. Trends Cogn Sci. 2010; 14:72–80. [PubMed: 20080054]

Vervaeke K, Lorincz A, Gleeson P, Farinella M, Nusser Z, Silver RA. Rapid Desynchronization of an Electrically Coupled Interneuron Network with Sparse Excitatory Synaptic Input. Neuron. 2010; 67:435–451. [PubMed: 20696381]

Vogels TP, Abbott LF. Gating multiple signals through detailed balance of excitation and inhibition in spiking networks. Nat Neurosci. 2009; 12:483–491. [PubMed: 19305402]

Vogelstein JT, Packer AM, Machado TA, Sippy T, Babadi B, Yuste R, Paninski L. Fast nonnegative deconvolution for spike train inference from population calcium imaging. J Neurophysiol. 2010; 104:3691–3704. [PubMed: 20554834]

Wang Y, Toledo-Rodriguez M, Gupta A, Wu C, Silberberg G, Luo J, Markram H. Anatomical, physiological and molecular properties of Martinotti cells in the somatosensory cortex of the juvenile rat. J Physiol. 2004; 561:65–90. [PubMed: 15331670]

Waters J, Helmchen F. Background synaptic activity is sparse in neocortex. The Journal of neuroscience : the official journal of the Society for Neuroscience. 2006; 26:8267–8277. [PubMed: 16899721]

Watson BO, MacLean JN, Yuste R. UP states protect ongoing cortical activity from thalamic inputs. PLoS One. 2008; 3:e3971. [PubMed: 19092994]

Woodruff A, Xu Q, Anderson SA, Yuste R. Depolarizing effect of neocortical chandelier neurons. Frontiers in neural circuits. 2009; 3:15. [PubMed: 19876404]

Xu H, Jeong HY, Tremblay R, Rudy B. Neocortical somatostatin-expressing GABAergic interneurons disinhibit the thalamorecipient layer 4. Neuron. 2013; 77:155–167. [PubMed: 23312523]

Xu X, Roby KD, Callaway EM. Immunochemical characterization of inhibitory mouse cortical neurons: three chemically distinct classes of inhibitory cells. J Comp Neurol. 2010; 518:389–404. [PubMed: 19950390]

Yuste R, Katz LC. Control of postsynaptic Ca2+ influx in developing neocortex by excitatory and inhibitory neurotransmitters. Neuron. 1991; 6:333–344. [PubMed: 1672071]

Yuste R, Peinado A, Katz LC. Neuronal Domains in Developing Neocortex. Science. 1992; 257:665–669. [PubMed: 1496379]

HHMI Author Manuscript
HHMI Author Manuscript
HHMI Author Manuscript



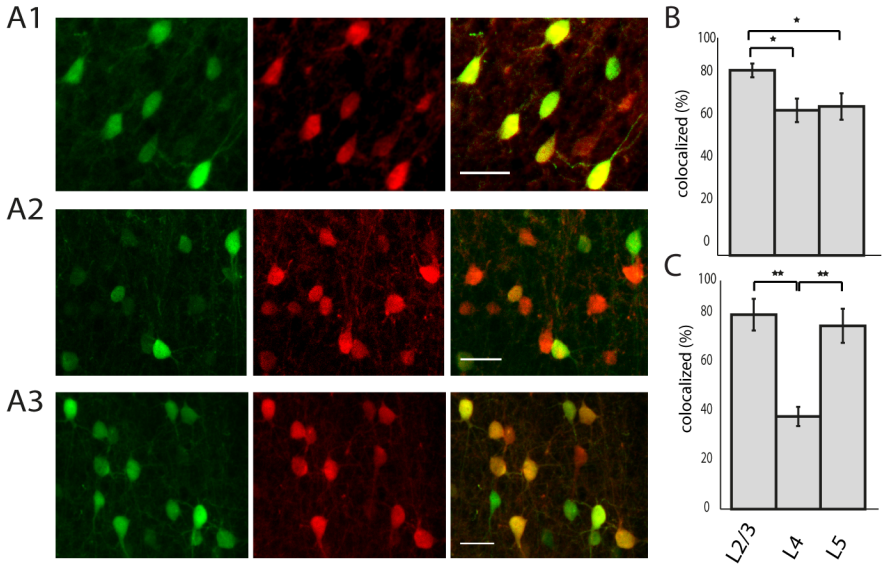


**Figure 1. Layer-specific colocalization of GFP and PV in G42 animals.** ***A1-A3***
Cortical S1 was double labeled for GFP and PV. Left panel (green) shows antibody labeling for GFP, middle column shows PV immuno-labeling (red), and far right column is the overlay. Top row is L2/3, middle row is L4, and bottom row is L5. Scale bar: 30μm. ***B*** the percentage of GFP positive cells that were also positive for PV was significantly higher in layer 2/3 than either layer 4 or 5 ($p < 0.01$, one way ANOVA). ***C*** The percentage of PV cells that were labeled for GFP was significantly lower in L4 than either layer 2/3 or 5 ($p < 0.001$, one-way ANOVA).

HHMI Author Manuscript
HHMI Author Manuscript
HHMI Author Manuscript



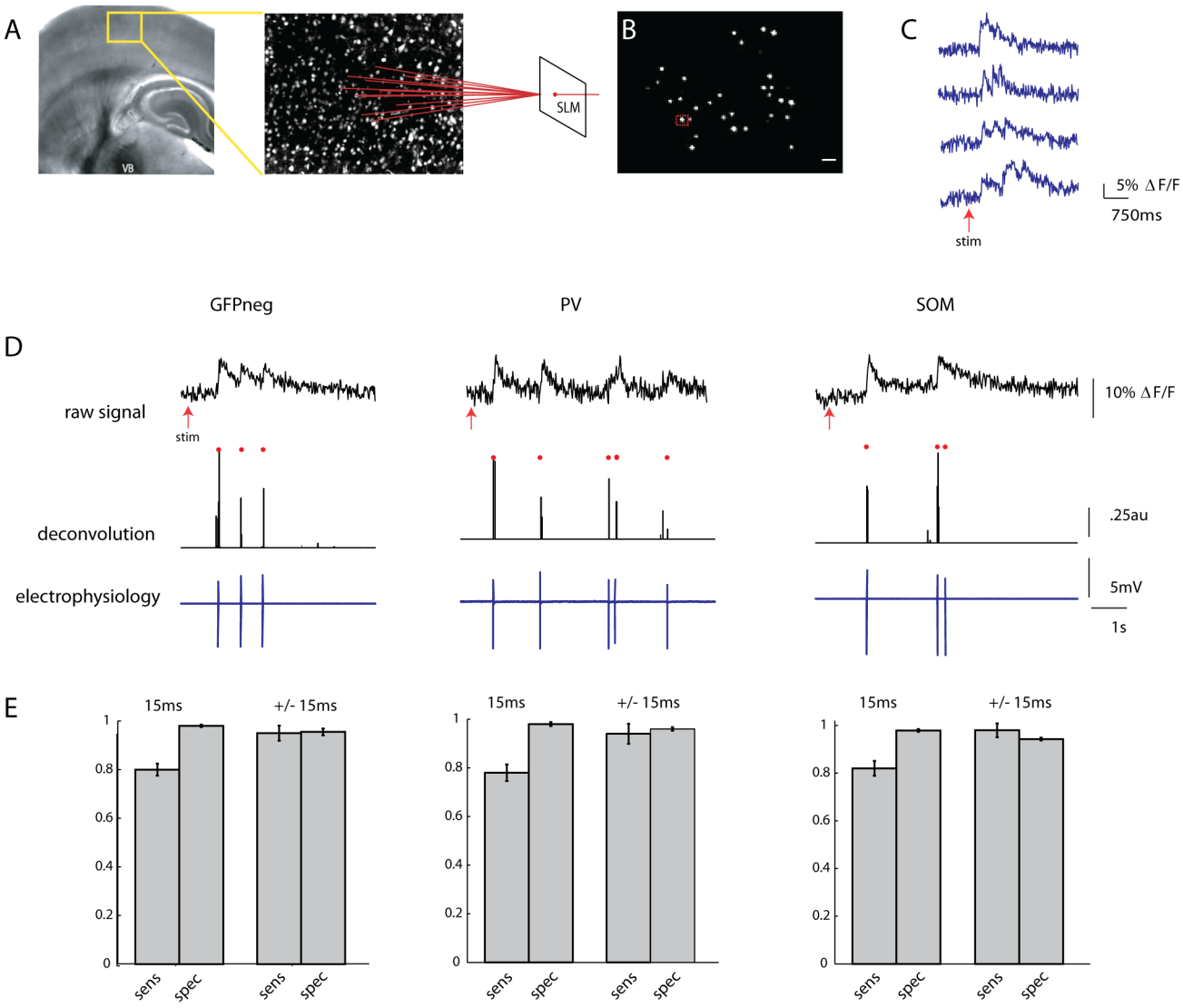


**Figure 2. Two photon fast calcium imaging with a single spike deconvolution algorithm**

***A,*** Light micrograph of a somatosensory (S1) thalamocortical slice preparation with intact thalamic input nucleus (ventrobasal nucleus, VB), thalamocortical axons and the somatosensory cortex. A stimulating electrode is placed in VB. Superimposed yellow box indicates location, over layers 2/3 and 4, of illustrated two photon z stack to right. Neurons pictured in this field are loaded with fura-2 AM dye, and targeted with a spatial light modulator (SLM, far right). ***B,*** Two photon image of a single frame showing neuronal cell bodies targeted with two photon illumination with the SLM. Cell outlined in red was targeted in cell-attached mode (scale bar 30μm), and is shown in D. Scale bar is 30μm ***C,*** Examples of fluorescence signals showing changes in fluorescence, normalized to baseline (ΔF/F), from four cells imaged at 66.6 Hz with an EMCCD. ***D,*** Three examples from calibration experiments in which a PC (left), a PV cell (middle) and SOM cell (right) were targeted for cell attached recording during simultaneous stimulation of the thalamus. Top trace shows raw fluorescence signal from that cell imaged at 66.6 Hz. Middle trace is the deconvolution of the calcium signals using parameters obtained from electrophysiology to obtain estimated spike times. Red dots above both traces indicate the time of the actual spikes. Bottom trace shows the associated electrophysiological trace. ***E,*** Sensitivity (true

positive rate) and specificity (1-false positive rate) of the deconvolution algorithm. These rates were calculated while allowing for either no window around each spike to search for a signal (“15ms”), or for a window of +/− 1 frame around each spike (“+/− 15ms”).

HHMI Author Manuscript HHMI Author Manuscript HHMI Author Manuscript

HHMI Author Manuscript
HHMI Author Manuscript
HHMI Author Manuscript



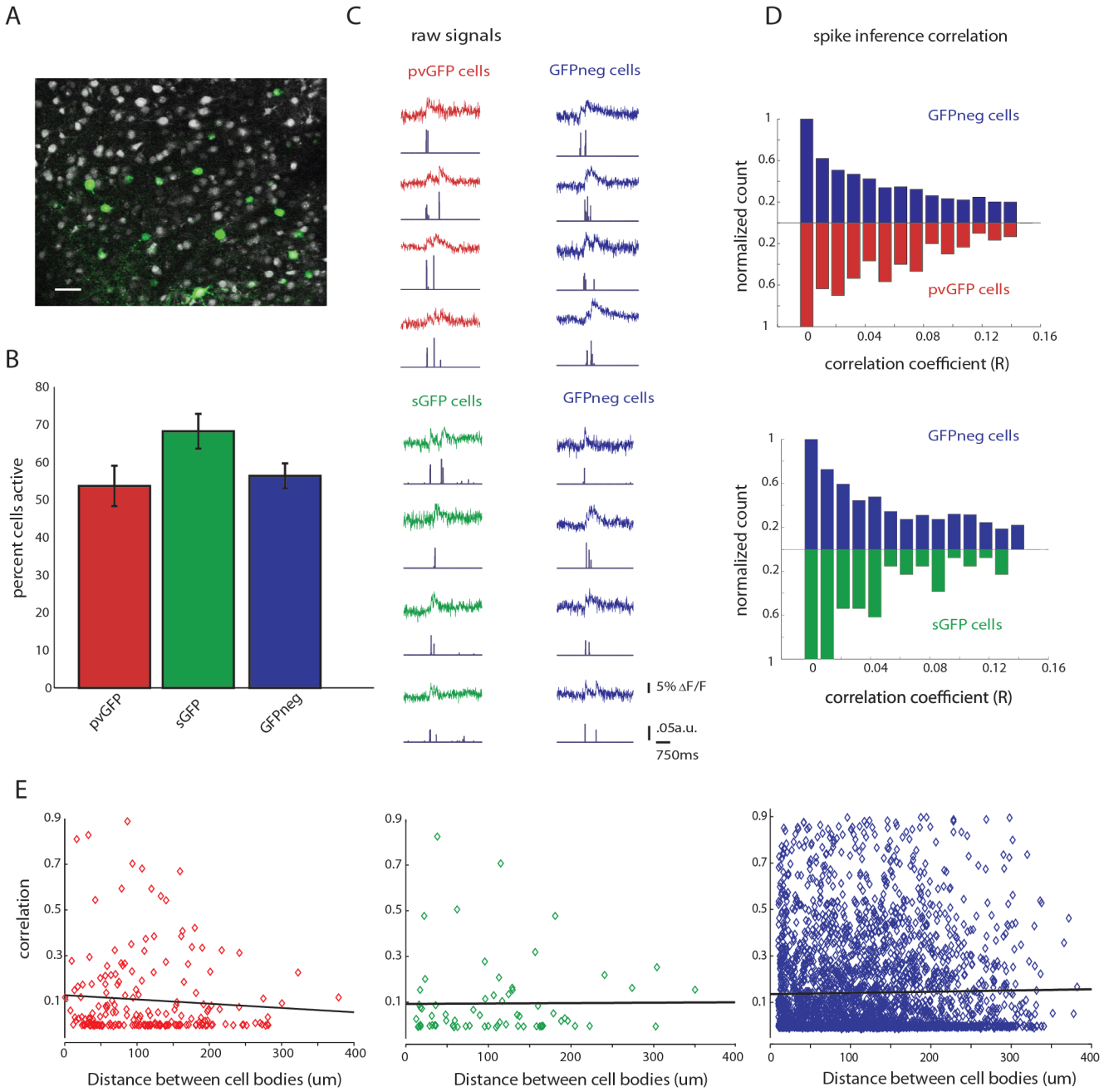


**Figure 3. Interneurons are weakly correlated during thalamically triggered activity**

***A,*** Two-photon image of a loaded slice with labeled interneurons (pvGFP) pseudocolored in green, scale bar 30μm. ***B,*** Quantification of the average percent active pvGFP (red), sGFP (green), and GFPneg (blue) neurons as determined by SLM imaging and deconvolution. ***C,*** Example fluorescence traces from simultaneously imaged pvGFP and GFPneg cells (top) or sGFP cells and GFPneg cells (bottom) during a thalamically triggered UP state. Spike inference for each trace is shown below each example. ***D,*** Normalized distribution of correlation coefficients of spike inference for pvGFP interneurons and GFPneg cells (top) and sGFP interneurons and GFPneg cells (bottom). These distributions were not significantly different (Friedman test, p = .2874). ***E***, Distance vs. correlation for all cell pairs

imaged. No significant relationship was found between distance and strength of correlation for pvGFP cells (left, p = 0.27), sGFP cells (middle, p = 0.78) or GFPneg cells (right, p = 0.27) .

HHMI Author Manuscript
HHMI Author Manuscript
HHMI Author Manuscript

HHMI Author Manuscript
HHMI Author Manuscript
HHMI Author Manuscript



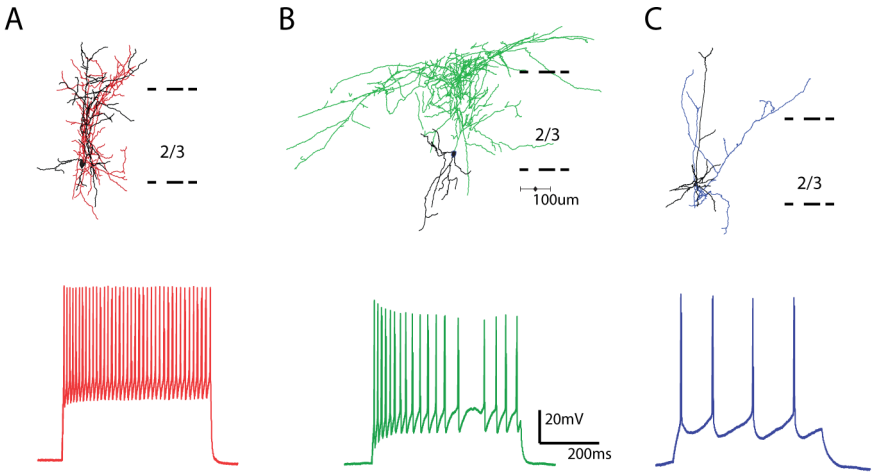


**Figure 4. Morphological and physiological characterization of interneurons**

***A***, Reconstruction of a PV GFP positive basket cell (top), with typical fast spiking physiology (below). Axons in red, dendrites in black. ***B,*** Reconstruction of a SOM GFP positive martinotti cell, with typical accommodating firing pattern shown below. Axons in green, dendrites in black. ***C***, Reconstruction of a layer 2/3 PC, with characteristic regular firing pattern shown below. Axons in blue, dendrites in black.

HHMI Author Manuscript
HHMI Author Manuscript
HHMI Author Manuscript



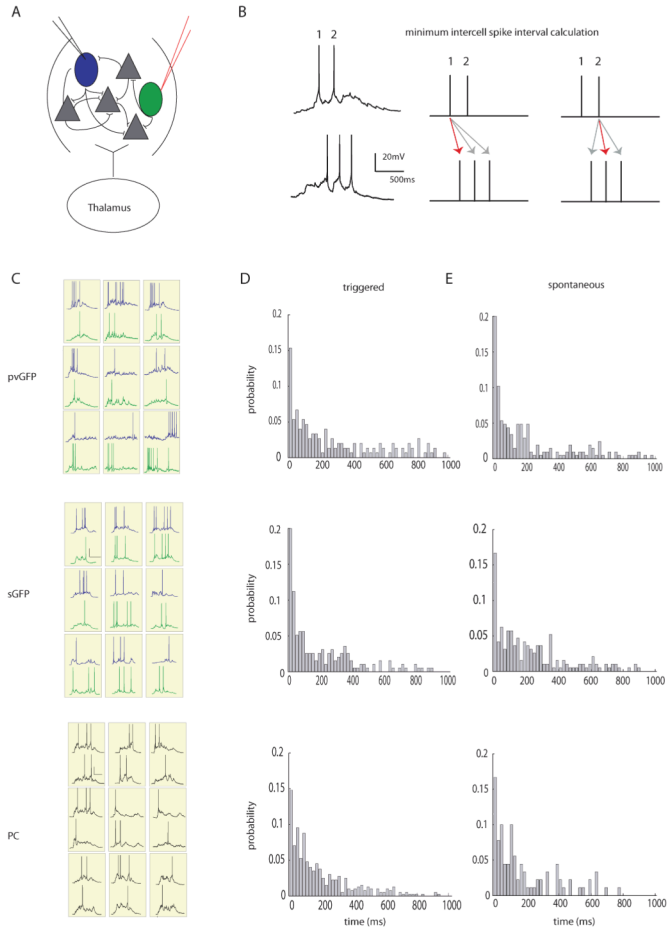


**Figure 5. Spiking of interneuron subtypes is not more synchronous than pyramidal cells**

***A,*** Cartoon depicting a layer 4 small recurrent network of cells consisting of interneurons (green and blue) and principal cells (gray). Two nearby cells, either pvGFP, sGFP, or unlabeled principal cells (PC) were patched in whole cells current clamp mode within 200μm of one another. ***B,*** Left, electrophysiological traces from two nearby sGFP cells. To the right, a schematic depicting how the minimum intercell spike interval was calculated for each spike in the top trace to the right. ***C,*** Representative traces from 9 pairs of simultaneously patched pvGFP (top), sGFP (middle), and PC (bottom) pairs during thalamic stimulation during trials in which both cells fired action potentials. ***D,*** Probability distributions of minimum intercell spike time intervals for pvGFP cells, sGFP cells and PCs during thalamic stimulation were not significantly different from one another (Friedman test, $p = 0.5874$) ***E,*** Probability distributions of minimum inter-cell spike time intervals during spontaneously occurring activations were not significantly different from one another (Friedman test $p = 0.08$) .

HHMI Author Manuscript
HHMI Author Manuscript
HHMI Author Manuscript

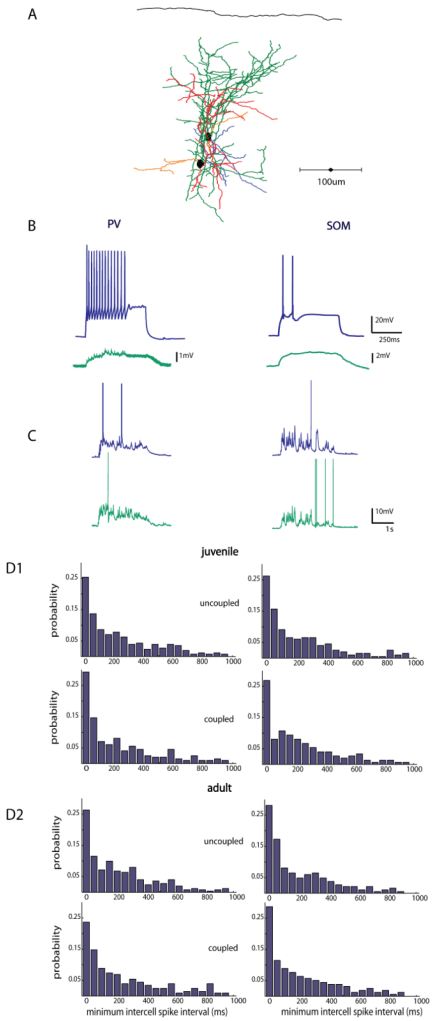


**Figure 6. Electrical coupling does not influence synchrony of interneurons**

***A,*** Anatomical reconstruction of 2 pvGFP cells patched within 60μm of one another that were gap junction coupled (axons of cell 1 are in green, dendrites in red, Axons cell 2 in blue, dendrites orange) ***B,*** Intracellular current injections in a PV neuron and a SOM neuron at 2x rheobase (blue traces top), with a nearby electrically coupled neuron patched within 100μm (green traces, bottom). ***C,*** Representative traces from a pair of PV interneurons, and SOM interneurons, respectively, in response to thalamic stimulation. ***D,*** Distribution of minimum spike times in PV (left) and SOM (right) interneurons in ***1,*** juvenile and ***2,*** adult animals. Mean minimum intercell spike time distributions did not differ between uncoupled and coupled neurons in either juvenile or adult slices

HHMI Author Manuscript
HHMI Author Manuscript
HHMI Author Manuscript



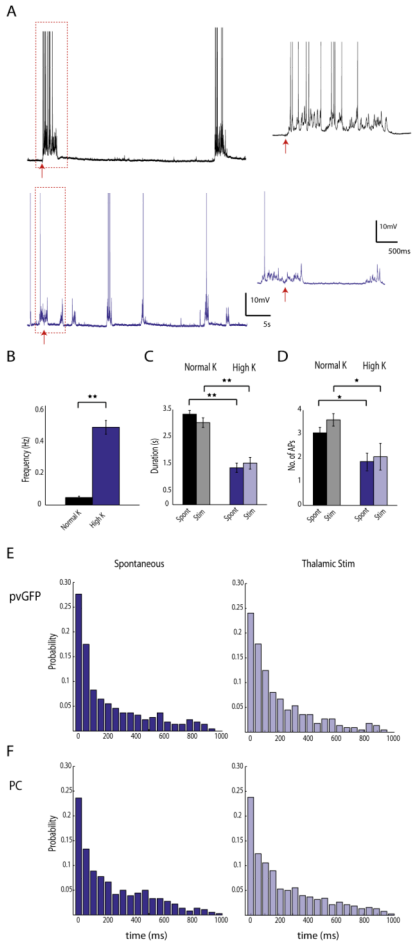


**Figure 7. Interneurons are not synchronous during low frequency oscillations**

***A***, Thalamic activation of cortical neurons in two different UP states regimes. Recordings were made from pvGFP interneurons and PCs in ACSF with either normal $K^+$ (top trace, black) or high $K^+$ (bottom trace, purple). The thalamus was stimulated in both of these conditions, and the response to this stimulation is shown in the expanded traces to the right. ***B***, the frequency of UP states in high $K^+$ was significantly higher than normal $K^+$. ***C***. the duration of the UP state was significantly shorter in high $K^+$ vs. normal $K^+$ for both spontaneous ('spont') and thalamically stimulated ('stim') UP states. No significant difference was found when comparing spont vs. stim in either high $K^+$ or normal $K^+$. ***D***, the number of action potentials fired by PV cells and PCs during the UP state was significantly lower in high $K^+$ vs. normal $K^+$ for both spont and stim UP states. No significant difference was found when comparing spont vs. stim in either high $K^+$ or normal $K^+$. ** indicate significance $p < 0.001$, * indicates $p < 0.01$. ***E***, Distributions of minimum intercell spike intervals for pvGFP interneurons in high $K^+$ for both spont (left) and stim (right) conditions. F, Distributions of minimum intercell spike intervals for PCs in high $K^+$ for both spont (left) and stim (right) conditions. No significant difference was found when comparing pvGFP vs PC distributions in spont and stim conditions.

HHMI Author Manuscript
HHMI Author Manuscript
HHMI Author Manuscript



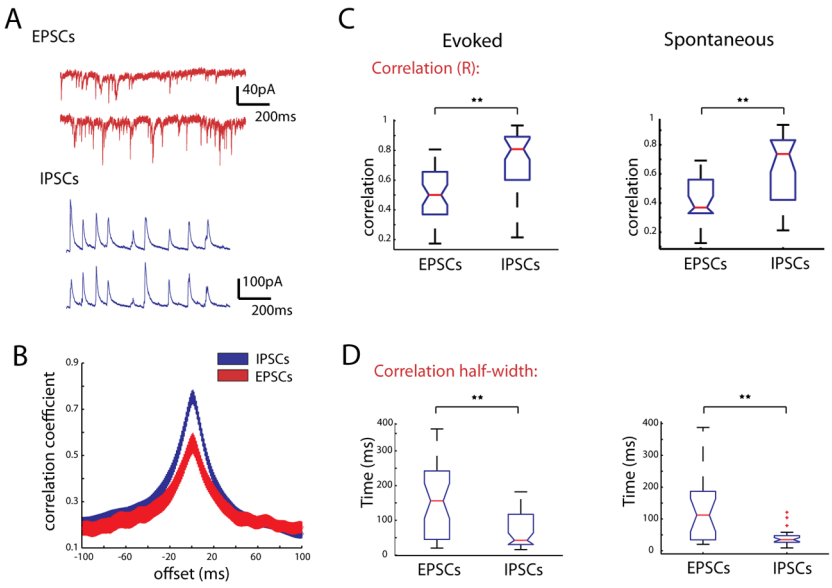


**Figure 8. IPSCs are more highly correlated than EPSCs during triggered and spontaneous activations**

***A,*** Recordings from two PCs with cell bodies ~68 μm apart. Top trace shows EPSCs during thalamic stimulation, bottom shows IPSCs recorded in the same cells on an alternate trial. ***B,*** Cross correlations between currents at 0mV (blue) and −70mV (red). ***C,*** Box plots of all correlation coefficients calculated for EPSCs recorded at −70mV and IPSCs recorded at 0mV during evoked activity (left) and spontaneous activity (right). ***D,*** Half width of the cross correlations for EPSCs and IPSCs. ** indicate a difference of significance with $p < 0.001$.

HHMI Author Manuscript
HHMI Author Manuscript
HHMI Author Manuscript



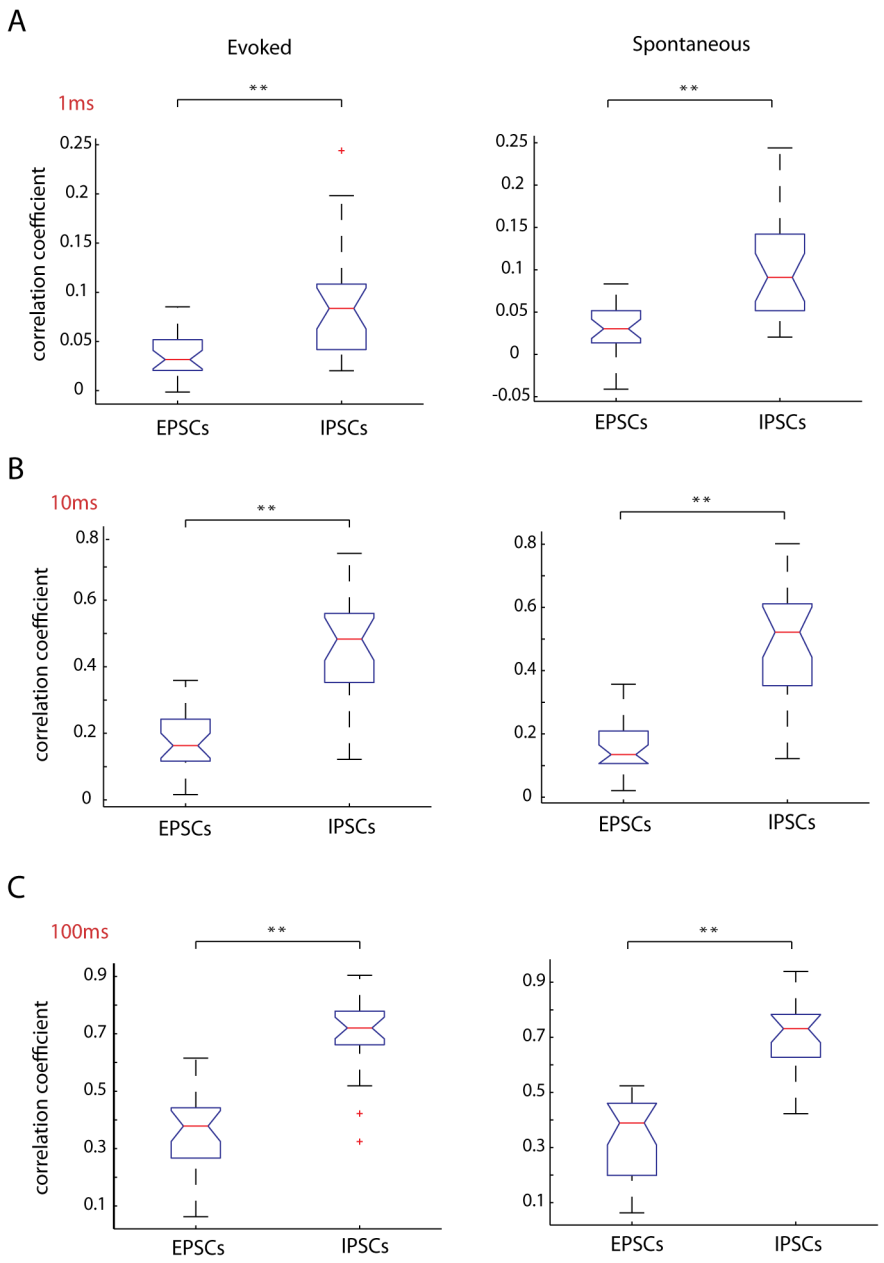


**Figure 9. Correlation of unitary EPSCs and IPSCs confirms IPSCs are more synchronous that EPSCs**

Individual IPSCs and EPSCs were detected and binary vectors of the event times were correlated among simultaneously patched cells pairs. These vectors were binned at either ***A***, 1ms, ***B,*** 10ms or ***C,*** 100ms. For all time bins, the correlation coefficient for IPSCs was significantly higher than EPSCs for both evoked and spontaneous activity. ** indicate a difference of significance with $p < 0.001$.

HHMI Author Manuscript
HHMI Author Manuscript
HHMI Author Manuscript



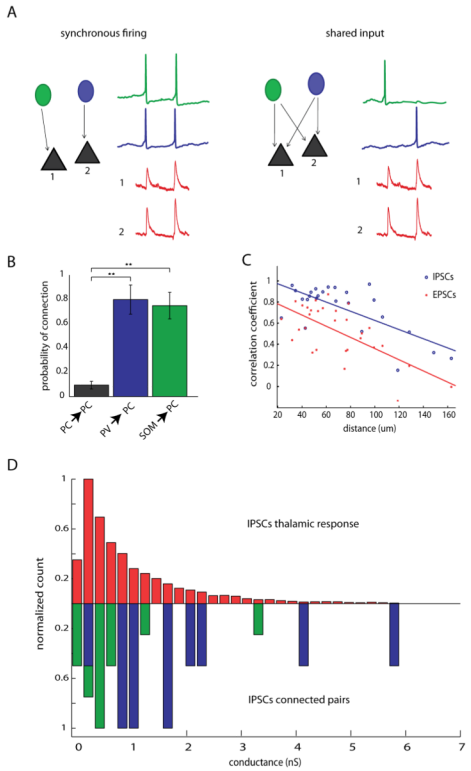


**Figure 10. High correlation of IPSCs is due to common input, rather than synchronous firing of interneurons**

***A,*** Schematic depicting two possible mechanisms underlying correlated IPSCs. In the first scenario, depicted to the left, “synchronous firing”, correlated IPSCs would be caused by two or more interneurons firing simultaneously. In this case, each IPSC would be the sum of the spiking of several interneurons. In the second scenario, “shared input”, in a system where every interneuron has highly divergent axons and contacts many postsynaptic PCs, each time an interneuron fires a spike, an IPSC would be recorded from all of its downstream postsynaptic targets nearly simultaneously. ***B,*** Connection probabilities for PC→PC pairs pvGFP→PC pairs and sGFP→PC pairs showing significantly higher connection probability for interneuron→PC than for PC→PC (p = 0.001 Kruskal Wallis; $p < 0.001$ for PC vs pvGFP and PC vs sGFP; $p > 0.05$ for pvGFP vs sGFP, Dunn’s multiple-comparison test), ** signifies significance p < 0.01) ***C,*** Distance vs. correlations coefficients of IPSCs (blue circles) and EPSCs (red crosses) were plotted for all cell pairs. Both EPSC and IPSC correlations drop off with distance with slopes that were not significantly different from one another (analysis of covariance p = 0.52). ***D,*** Normalized distribution of conductances for IPSCs recorded during thalamically triggered activations (top, red), and synaptic conductances measured from pvGFP→ PC pairs (blue) or sGFP→ PC pairs (green). The mean of these distributions did not differ from one another (p = 0.442, Mann-Whitney).

HHMI Author Manuscript
HHMI Author Manuscript
HHMI Author Manuscript



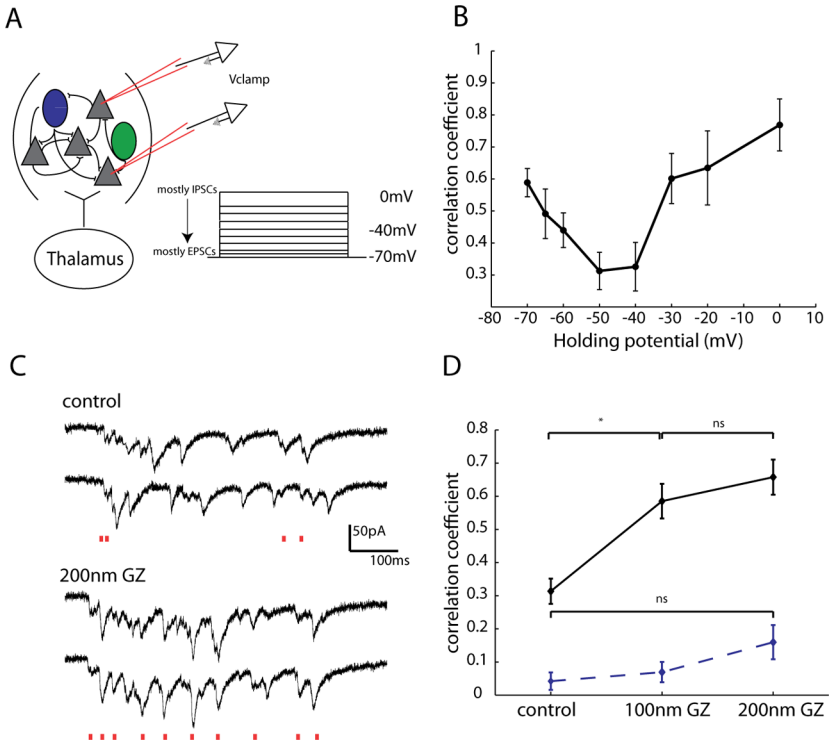


**Figure 11. Pharmacologically decreasing inhibition decorrelates excitation**

**A,** Schematic showing experimental configuration. Two excitatory cells were patched within 100μm of one another while a thalamically triggered UP state was simultaneously recorded in the two cells at different holding potentials ranging from 0mV (mostly IPSCs) to −70mV (mostly EPSCs), with a mixture of IPSCs and EPSCs recorded at intermediate potentials. **B,** The correlation coefficient was calculated for EPSCs at these different hold potentials. Starting from −70mV, correlation values decreased, hitting their lowest value at intermediate potentials, and increasing again as holding potential approached 0mV. ***C,*** Example traces from two PCs recorded 55μm from one another. These two cells were voltage clamped at −70mV so EPSCs could be recorded. Above traces are control, and below in 200nm gabazine (GZ). Red lines below each set of traces indicated EPSCs in both cells that occurred within 10ms of one another. ***D,*** Nanomolar concentrations of gabazine (GZ) significantly increased correlations in EPSCs ($p < .05$, significance indicated by *, Mann-Whitney, n = 5 pairs). Dashed line shows correlation of shuffled data, which did not differ significantly between control and either 100nm or 200nm GZ.

HHMI Author Manuscript
HHMI Author Manuscript
HHMI Author Manuscript



**Table 1**

Electrophysiological properties of pvGFP, sGFP and PC cells

| | pvGFP | sGFP | PC |
|---|---|---|---|
| **Number of cells** | 42 | 50 | 62 |
| **Input Resistance (MΩ)** | 225 ± 29.0 | 400 ± 88.9 | 542 ± 76.3 |
| **AP half width (ms)** | .712 ± 0.07 | 1.05 ± 0.09 | 1.65 ± 0.13 |
| **Resting membrane potential (mV)** | −70.6 ± 1.27 | −67.8 ± 0.92 | −71.5 ± 0.82 |
| **Rheobase (pA)** | 218.6 ± 31.78 | 148.4 ± 25.25 | 51.1 ± 9.15 |
| **Firing frequency at 2x threshold (Hz)** | 65.0 ± 9.04 | 24.9 ± 3.14 | 11.0 ± 0.82 |
| **Spike Frequency Adaptation** | 0.79 ± 0.03 | 0.41 ± 0.04 | 0.72 ± 0.04 |

HHMI Author Manuscript

HHMI Author Manuscript

HHMI Author Manuscript

**Table 2**

Similar properties of IPSCs for monosynaptic connections and UP states

| | IPSCs pairs (n =25) | IPSCs UP state (n = 6578) | Statistics |
|---|---|---|---|
| **10–90 Rise time (ms)** | 3.11 ± 0.37 | 3.67 ± 0.24 | ns |
| **Amplitude (pA)** | 97.53 ± 21.06 | 77.14 ± 8.81 | ns |
| **Half-width (ms)** | 15.98 ± 0.98 | 13.76 ± 0.84 | ns |
| **Decay constant (ms)** | 19.10 ± 1.45 | 17.50 ± 1.94 | ns |